ChemComm

Precision Synthesis of Linear Oligorotaxanes and Polyrotaxanes Achieving Well-Defined Positions and Numbers of Cyclic Components on the Axle

Journal:	*ChemComm*
Manuscript ID	CC-FEA-06-2021-003507.R2
Article Type:	Feature Article

FEATURE ARTICLE

Precision Synthesis of Linear Oligorotaxanes and Polyrotaxanes Achieving Well-Defined Positions and Numbers of Cyclic Components on the Axle

Received 00th January 20xx,
Accepted 00th January 20xx

DOI: 10.1039/x0xx00000x

Hiroshi Masai,* Yuki Oka, and Jun Terao*

Interest in macromolecules has increased because of their functional properties, which can be tuned using precise organic synthetic methods. For example, desired functions have been imparted by controlling the nanoscale structures of such macromolecules. In particular, compounds with interlocked structures, including rotaxanes, have attracted attention because of their unique supramolecular structures. In such supramolecular structures, the mobility and freedom of the macrocycles are restricted by an axle and dependent on those of other macrocycles, which imparts unique functions to these threaded structures. Recently, methods for the ultrafine engineering and synthesis, as well as functions, of "defined" rotaxane structures that are not statistically dispersed on the axle (i.e., control over the number and position of cyclic molecules) have been reported. Various synthetic strategies allow access to such well-defined linear oligo- and polyrotaxanes, including [1]rotaxanes and [*n*]rotaxanes (mostly $n > 3$). These state-of-the-art synthetic methods have resulted in unique functions of these oligo-and polyrotaxane materials. Herein, we review the effective synthetic protocols and functions of precisely constructed one-dimensional oligomers and polymers bearing defined threaded structures, and discuss the latest reports and trends.

1. Introduction

Techniques for the precise control of the chemical structures of macromolecules to achieve characteristic and precisely engineered properties have been intensively developed in recent years. In particular, interlocked supramolecular structures, including rotaxanes and catenanes, have unique features and functions resulting from their nanostructures, specifically their mechanically connected cyclic and axle components.[1–6] For example, in rotaxanes, an axle molecule is threaded through cyclic molecules, and these have been applied as stimuli-responsive units because the cyclic molecules can move along the axle (shuttling) on the application of weak chemical or physical stimuli.[7–9] This intriguing behavior has resulted in extensive investigations into polymeric rotaxane structures.[10,11] In particular, since Harada et al. reported effective synthetic procedures for polyrotaxanes consisting of poly(ethylene glycol) and cyclodextrins,[12–15] numerous polyrotaxanes have been developed containing various types of cyclic and axle molecules.[16–22] These polyrotaxanes have unique functions based on the shuttling of macrocycles induced by thermal and chemical stimuli.[23] For instance, Ito et al. demonstrated that polyrotaxane-based soft materials have high toughness and elasticity, suggesting their suitability for industrial applications.[24–26] Moreover, in polyrotaxanes composed of π-conjugated polymer backbones, the cyclic molecules inhibit π–π interactions between conjugated chains, thus improving the physical properties related to the π-system.[27–29] These examples demonstrate the interesting features of polyrotaxanes with respect to both fundamental science and industrial applications.[30,31]

It has been a few decades since the first efficient synthesis of polyrotaxanes was reported,[12] and recent research has shifted its focus to innovative synthetic procedures towards such materials and their applications.[31] In particular, the ultrafine engineering and functions of rotaxane structures have been reported along with the development of synthetic methodologies for the preparation of "defined threaded structures," in which the number and position of the cyclic molecules on the axle can be precisely defined. In this *Feature Article*, we review effective synthetic methodologies for forming defined rotaxane structures from one-dimensional oligomers and polymers. We also discuss the functions of defined rotaxanes provided by their precise engineering, as well as recent reports and trends.

[a] *Department of Basic Science, Graduate School of Arts and Sciences, The University of Tokyo, Japan.*
E-mail: cmasai.h@g.ecc.u-tokyo.ac.jp, cterao@g.ecc.u-tokyo.ac.jp

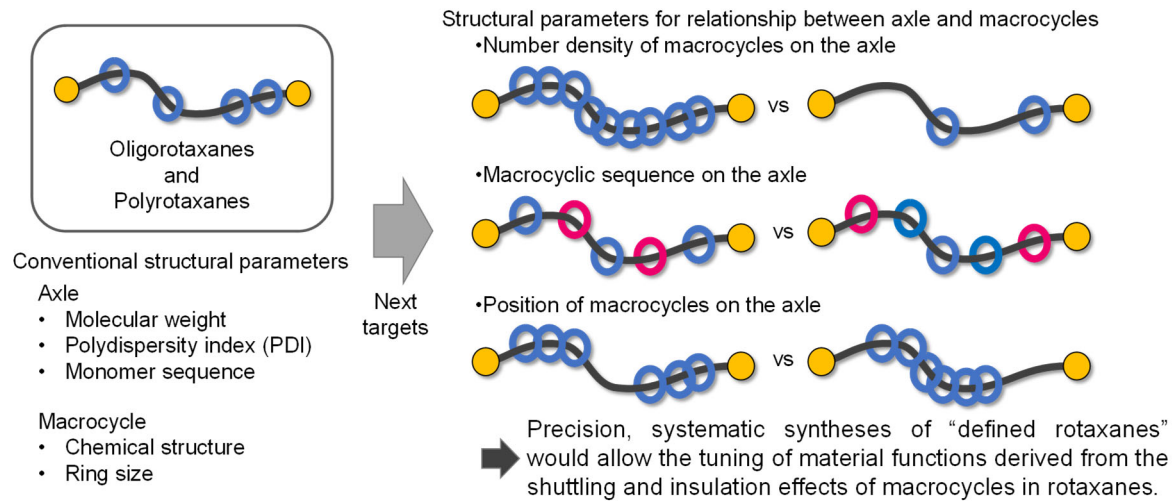

Fig. 1 Structural parameters affecting the material properties of rotaxanes based on oligorotaxanes and polyrotaxanes. Classification of conventional and recent target parameters.

2. Structural parameters of rotaxanes

The unique characteristics of rotaxanes, including oligorotaxanes and polyrotaxanes, are derived from their threaded supramolecular structures involving axle and cyclic molecules. Hence, their physical properties and functions can be attributed to their supramolecular structural parameters, including the number densities and positions of the cyclic molecules on the axle units, as well as the chemical structures of the axle and cyclic components, and the molecular weight of the axle; these are more conventional structural parameters (Fig. 1). For example, when polyrotaxanes possess a small number of macrocycles (i.e., have low coverage, where coverage = the ratio of cyclic molecules on the axle), their cyclic components will exhibit high mobilities, which can enhance their functional properties based on shuttling.[32,33] In contrast, the shuttling effects of polyrotaxanes with large numbers of macrocycles (i.e., high number densities) are minimized owing to the limited molecular interactions between their axles and the steric hindrance between adjacent cyclic molecules on their axles. Hence, the amount of macrocycles on the axles of these unique supramolecular structures is a fundamental factor governing their functionalization. In general, polymers and oligomers having defined molecular weights, monomer sequences, and stereoregularities of their backbones have excellent material properties owing to their fine-tuned structures, which are controlled using iterative reactions, homo- and heterogeneous catalysis, and living polymerization.[34–36] Thus, the concepts related to the precision engineering of macromolecules used to achieve promising material functions could be applied to rotaxane-type macromolecules. Alongside molecular weight, polydispersity index (PDI), and polymer sequences, the control over the numbers and positions of cyclic molecules in rotaxane-based oligomers and polymers is also important for the precision synthesis of polymers; it would enable the fine tuning of the functions derived from the associated shuttling and insulation effects of rotaxane structures. However, such supramolecular structural parameters are thermodynamically determined by the supramolecular interactions between the macrocycles and the axles.[37] Hence, in general, the structural parameters of polyrotaxanes, including the numbers and positions of the cyclic molecules on their axles and their axle polymer lengths, are statistically dispersed. As a result, the precise control of these parameters remains challenging.

The synthetic strategies for preparing supramolecular threaded structures (e.g., rotaxanes) have been developed for over 50 years. The initial synthetic methods towards rotaxanes only achieved extremely low yields (< 1%) because the thread formations in the solutions of rotaxane precursors were problematic.[38] In the 1980s, template methodologies were developed to synthesize rotaxane structures more effectively, resulting in yields of a few dozen percent to quantitative yields. These methods focused on utilizing metal coordination, hydrogen bonding, and electrostatic interactions.[39–41] These highly effective template-based synthetic strategies laid the groundwork for the development of rotaxane-based materials containing a wider range of molecules, such as oligomers and polymers.[42] These advancements have led to investigations into the precision syntheses of [2] and [3]rotaxanes.[43] However, examples of the precision synthesis of [*n*]rotaxanes drastically decrease as the number of components (i.e., *n*) increases.[44] Similarly, rotaxanes with a large number of cyclic components typically contain polydisperse numbers of cyclic molecules and various axle molecular weights. In particular, the number density of cyclic components on the axle is widely dispersed in conventional polyrotaxanes because the self-assemblies of the polymer and monomer are governed by thermodynamic equilibrium. Furthermore, during polyrotaxane syntheses, the self-assembled complexes of cyclic molecules on the axles can dissociate, thus yielding a statistical dispersion in the number density of cyclic molecules on the axle; this acts as a structural defect in the resultant polyrotaxanes.[20] Consequently, the next challenge facing the production of functional rotaxane-based materials is the precision synthesis of oligorotaxanes and polyrotaxanes with defined structural parameters but no

statistical dispersion. Herein, we categorize the synthetic strategies and functionalities of well-defined linear oligo- and polyrotaxanes, focusing on three key structural parameters: the number density, sequence, and positions of the cyclic components.

3. Fine control of the number density and sequence of cyclic molecules

One methodology to define the number of cyclic molecules possessed by rotaxanes was achieved using axle molecules with defined numbers of stations. A station is a point on the axle where favorable supramolecular interactions with the cyclic components can occur. Because each station interacts with one cyclic molecule, the resultant rotaxanes contain a defined number of macrocycles on their axles.[45–48] For example, in 2007, Wu and Stoddart et al. reported the effective synthesis of oligorotaxanes composed of oligoether-type macrocycles and axles bearing dialkylammonium cations.[49] They first synthesized axle **1** (Fig. 2a) as a rotaxane precursor with a defined number of ammonium cations as interaction points for macrocycles. Then, after the self-assembly of the macrocycle around each ammonium cation on the axle, they utilized a reversible imine formation to close the cycle and achieve a structurally well-defined rotaxane. Further, the dynamic covalent imine bonds improved the synthetic efficiency despite the large number of macrocycles. Typically, the synthesis of [*n*]rotaxanes bearing large numbers of macrocycles can be used to address the defects of the cyclic components themselves. In addition, the reversibility of the assembly process based on dynamic covalent imine bonds affords a thermodynamically stable species, where the ammonium cations interact with oligoether-type macrocycles without any macrocyclic defects. Hence, the synthetic strategy provided various oligorotaxanes (**2**), including [3], [4], [5], [7], and [11]rotaxanes, with well-defined numbers of macrocycles. In 2012, Stoddart et al. further improved the methodology for oligorotaxane synthesis.[50] In addition to dynamic covalent bonds, they implemented π–π interactions between adjacent macrocycles during the self-assembling process, which increased the stabilities of the self-assembled structures and provided highly effective oligorotaxane syntheses (up to [20]rotaxanes in over 90% yield).

Stoddart et al. also reported the synthesis of oligorotaxane **3** using multiple donors based on 1,5-dioxynaphthalene (DNP) as the axle stations for cyclobis(paraquat-*p*-phenylene) acceptor rings (Fig. 2b).[51–54] The electron-poor viologen moieties in the rings were assembled on the electron-rich stations of the axle by donor–acceptor interactions. During this assembly, numbers of cyclic molecules different from the number of station units were introduced on the axle because the donor–acceptor complex between one DNP station and one macrocycle was supported by two additional stations on the chain. As a result, continuous donor–acceptor stacks were constructed between seven axle stations and four cyclic components to form foldamer structures, in which specific

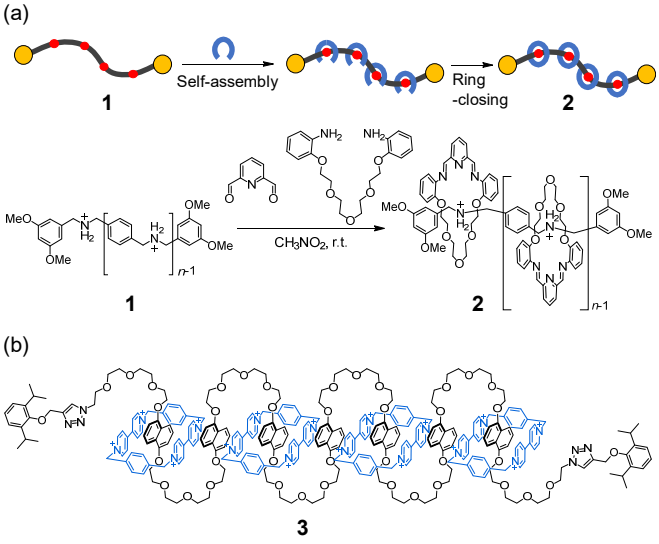

Fig. 2 (a) Schematic representation and synthesis of oligorotaxanes **2** utilizing multiple stations for macrocycles on the axle.[49] (b) Folded structure of oligorotaxane **3** based on donor–acceptor complexes.[51]

numbers of cyclic molecules preferentially assembled on the oligomer axle.

Furthermore, sequential control using multiple types of stations on the axle molecule allows the formation of sequence-defined oligorotaxanes with multiple macrocyclic components.[55–58] For example, Qu et al. combined axles **4** and **5** to synthesize a hetero[6]rotaxane containing three types of macrocycles (**6**–**8**) in a defined sequence on the combined axle molecule (Fig. 3).[59] Macrocycle **6** was found to encapsulate the viologen unit

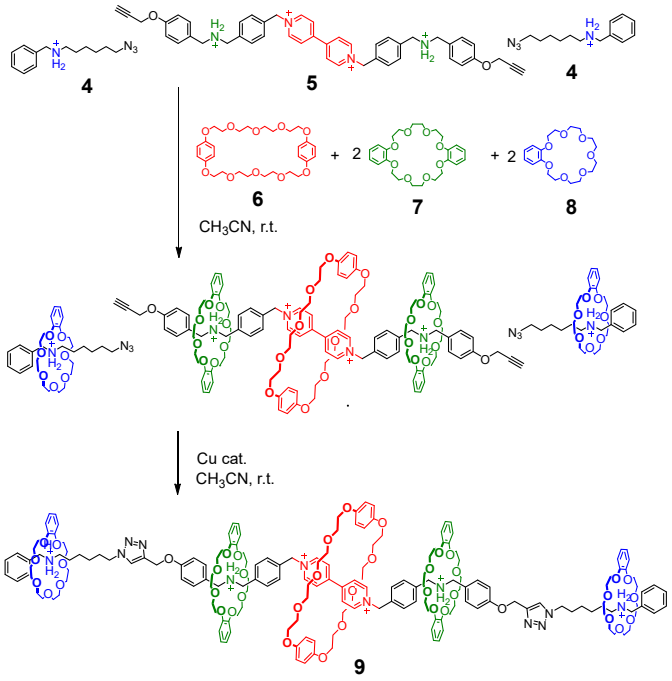

Fig. 3 Synthetic concept and route towards hetero[6]rotaxane **9** bearing three types of macrocycles, which proceeded via the self-assembly of multiple components.[59]

of axle molecule **5** more strongly than its dibenzylammonium unit owing to charge transfer and π–π interactions.[60] In addition, the binding target of macrocycle **8** was the sterically defined benzylalkylammonium cation of **4**, while macrocycle **7** selectively recognized the dibenzylammonium unit of **5** because the corresponding assembly would provide the largest binding constant among the three cation moieties.[55] This complementary association between the axle cation units and macrocycles **6**–**8** selectively afforded hetero[6]rotaxane **9**.

Another strategy for achieving a defined number and sequence of oligostructures is the iterative reaction methodology, which has been widely developed and utilized in synthetic and materials chemistry (Fig. 4a).[61–65] These iterative strategies have also been applied to give rotaxane structures with multiple cyclic components. Vögtle et al. reported an early example of the iterative method to synthesize oligorotaxanes in 1999.[66,67] They applied stepwise reactions to prepare an axle molecule bearing a bulky capping moiety. The oligorotaxanes were then synthesized by exploiting the hydrogen bonding between the macrocycles and amide moieties of the axle components.

In addition, Leigh et al. achieved the sequential synthesis of oligorotaxanes via metal-template methods using coordination sites on the axle molecule.[68] Specifically, they prepared an axle molecule (**10**) bearing a single pyridyl moiety as the coordination site for the template. Then, a Pd-bearing macrocycle was introduced onto the axle via coordination between the Pd(II) metal, the pyridyl moiety of **10**, and the macrocycle (Fig. 4b). Subsequent catalytic ring-closing metathesis afforded a metalated [2]rotaxane structure, whose internal alkene then underwent reduction by a diimide generated from 2-nitrobenzenesulfonylhydrazide (NBSH). Subsequent demetallation afforded metal-free [2]rotaxane **11** in 62% total yield. Subsequently, iterative reactions were conducted to form [3]rotaxane and [4]rotaxane **12** in 79% and 68% yield, respectively. Through another iterative synthetic strategy, in 2010, Leigh et al. also succeeded in the sequential, controlled synthesis of [3]rotaxanes with multiple types of cyclic molecules (Fig. 5).[69] Two different macrocycles were introduced stepwise onto nonsymmetrical axle molecule **10**, providing [3]rotaxanes **13** and **13'** bearing different sequences of the same macrocycles, as determined by their order of addition. Further, this new strategy could be used to prepare pairs of stereoisomers of [3]rotaxanes by controlling the iterative reaction sequence.

Goldup et al. reported another iterative synthetic technique for constructing oligorotaxanes (Fig. 6a).[70] Using a terminal alkyne, copper-catalyzed active-template synthesis with macrocycles and an azido-functionalized capping moiety afforded an extended rotaxane with an additional macrocycle.[39,71] The deprotection of the resultant rotaxane yielded a terminal alkyne, which could be utilized as the reaction site for subsequent extension of the rotaxane. The iterative process allowed [*n*]rotaxanes to be converted to [*n* + 1]rotaxanes, up to [6]rotaxane **14**, in excellent yields (>90% for each process). Moreover, changing the macrocycle introduced in each step afforded hetero[4]rotaxanes (**15**) containing different cyclic molecules in a well-defined sequence on the axle (Fig. 6b). This synthetic strategy provided various oligorotaxanes with defined axle lengths and numbers of macrocycles.

Recently, oligorotaxanes bearing a defined number of macrocycles have been synthesized by precisely controlling the energy barriers for the threading of macrocycles on the axle. Using sequential reactions, the kinetic barriers for shuttling were raised and lowered and the thermodynamic stability of the interactions between cyclic molecules and multiple stations was modified. In 2017, Leigh et al. reported the synthesis of a[5]rotaxane via sequential pH control (Fig. 7).[72] Two types of

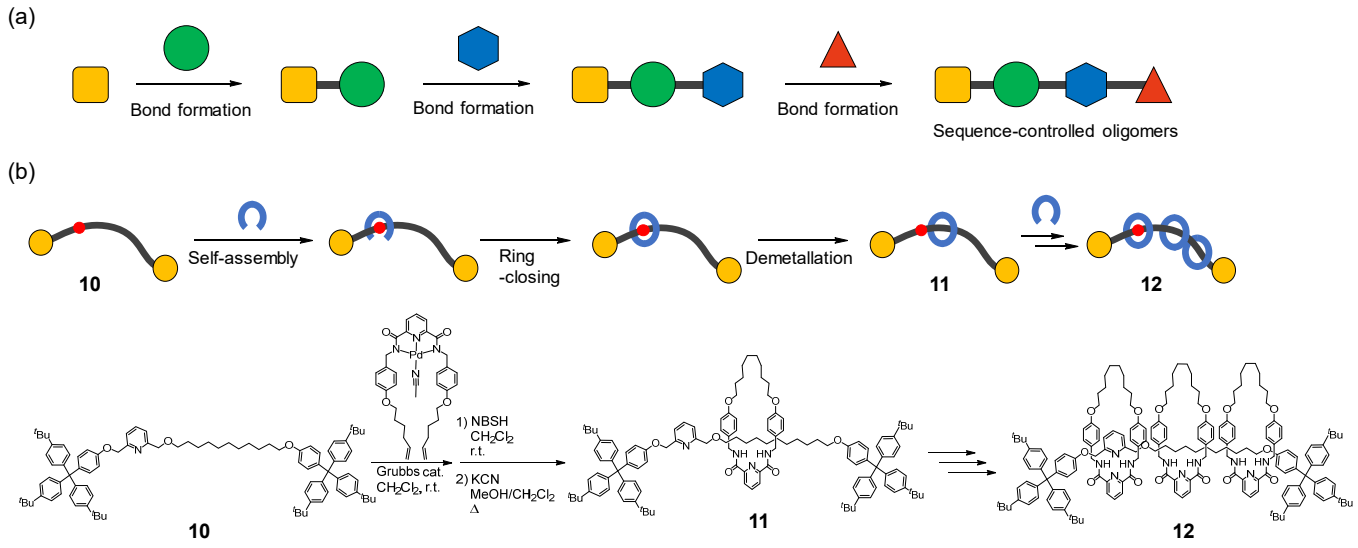

Fig. 4 (a) Schematic representation of the iterative protocol towards sequence-controlled oligomers. (b) Schematic representation and synthesis of oligorotaxanes **12** via the iterative introduction of cyclic molecules using a metal-template methodology.[68] NBSH: 2-Nitrobenzenesulfonylhydrazide.

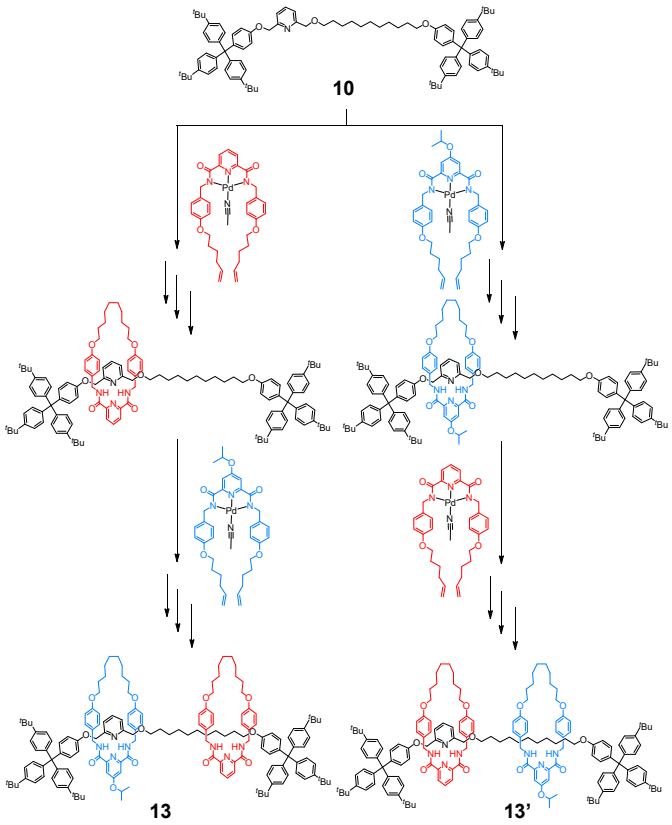

Fig. 5 Synthesis of [3]rotaxane stereoisomer pairs (**13** and **13'**) by controlling the order of addition of two kinds of cyclic molecules.[69]

stations, dibenzylammonium and triazolium cation moieties, were incorporated on axle molecule **16** for interactions with from threading onto the axle. Here, disulfide groups acted as a oligoether-type macrocycles. In addition, they combined two types of locking moieties on the axle to prevent macrocycles stable barrier under acidic conditions but a labile barrier under basic conditions. In contrast, the employed hydrazone groups are stable under basic conditions but labile under acidic conditions. That is, sequential shifts between acidic and basic conditions in the presence of additional thiol, disulfide, and hydrazide reagents allowed dynamic covalent bonds to be exchanged and the macrocycles to move from the outside of the axle to the inside. This stepwise threading mechanism was used with trichloroacetic acid, which underwent amine-catalyzed decarboxylation to produce $CHCl_3$ and CO_2. In this reaction system, in the presence of the amine, the acidic conditions induced by trichloroacetic acid gradually changed to basic conditions via the decomposition of the acid by the catalytic amine reagent. Thus, the sequential addition of the reagents, including trichloroacetic acid, induced the formation of oligorotaxane **17** after four cycles, which contained an average of 3.7 macrocycles. The strategy involves the use of molecular pumps, which enables thermodynamically unfavored products to be provided as out-of-equilibrium species through the utilization of chemical energy as fuels.[73]

Leigh et al. further developed molecular pumps toward the autonomous generation of [*n*]rotaxanes in 2021 (Fig. 8).[74] Amine-terminated axle **18** reacted with a 9-fluorenylmethyloxycarbonyl (Fmoc) derivative and crown ether to form [2]rotaxane **19** via a metal-free active-template method.[75] The cyclic molecule was initially located on the sterically crowded Fmoc-carbamate group, which thermodynamically passed over the trifluoromethyl group to form **19'**. Subsequently, the Fmoc group of [2]rotaxane **19'** was gradually deprotonated by an amine until decomposing into CO_2 and dibenzofulvene. Meanwhile, the Fmoc moiety of **19** was sterically protected by an adjacent macrocycle, resulting in the formation of amine-terminated [2]rotaxane **20**, wherein the cyclic molecule was kinetically trapped by the trifluoromethyl group on the axle. The process could be repeated by the continuous addition of the Fmoc derivative as chemical fuel, providing up to [4]rotaxane **21**. After the reaction, the Fmoc group present on the [4]rotaxane slowly decomposed under basic conditions, generating both the original axle (**18**) and various cyclic components as the lowest energy state. This

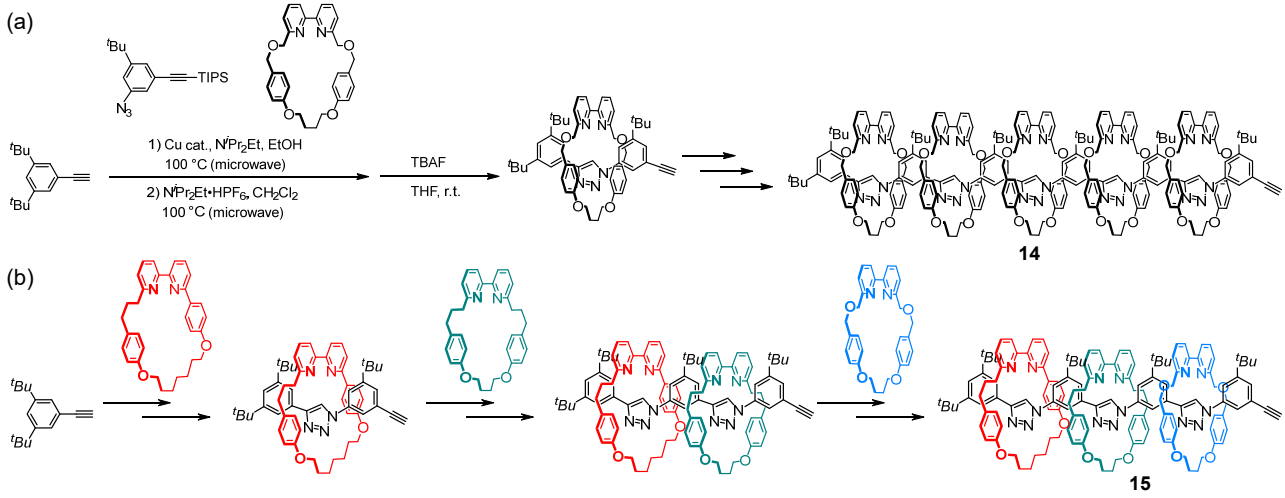

Fig. 6 Iterative syntheses of (a) [6]rotaxane **14** and (b) hetero-[4]rotaxane **15** having different macrocycles.[70]

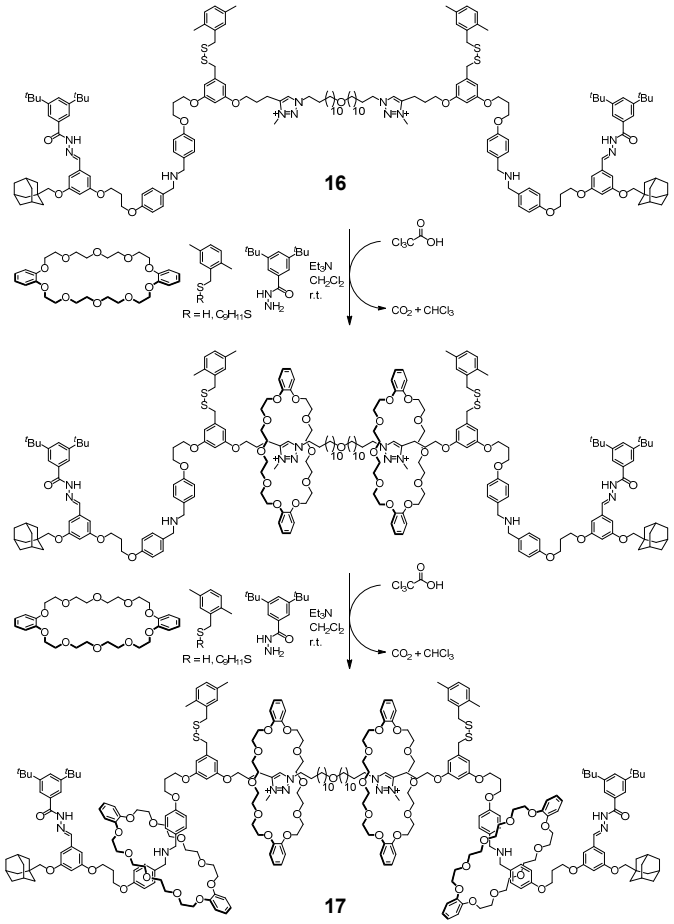

Fig. 7 Synthesis of oligorotaxane **17** bearing two types of locking moieties on its axle via acid/base cycles induced by the amine-catalyzed decarboxylation of trichloroacetic acid.[72]

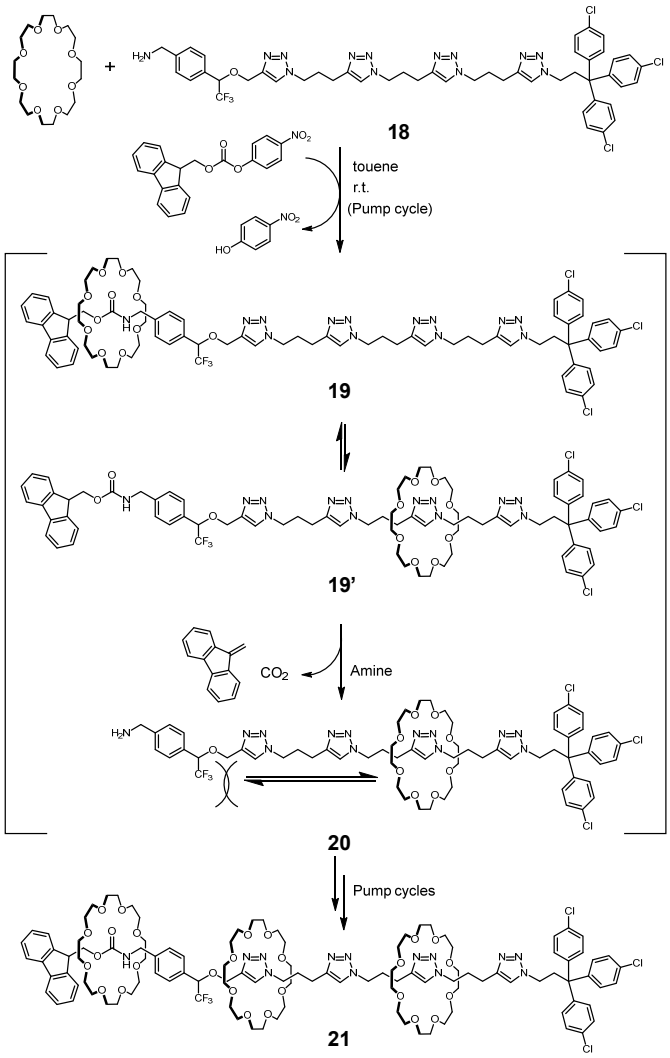

Fig. 8 Autonomous synthesis of [4]rotaxane **21** via molecular pumping by continuous addition of chemical fuel.[74]

confirms that [4]rotaxane **21** was obtained as a dissipative out-of-equilibrium species[76] via molecular pumps employing a chemical fuel.

These precision synthetic methodologies for rotaxane preparation have also been applied to macromolecular axles, and a defined number of macrocycles can be introduced to polymer chains composed of large numbers of repeating units. Stoddart et al. developed a iterative synthetic procedure for polyrotaxanes bearing defined numbers of macrocycles on polymeric axles via chemical or electrochemical redox cycles of cationic macrocycles and axles (Fig. 9).[77] Both ends of the ethylene glycol chain were capped with redox-inactive bulky units, redox-active cationic units, and then redox-inactive cationic units; this order was relative to the axle interior (**22**). They demonstrated stepwise redox processes providing poly[*n*]rotaxanes with a defined number of cyclic molecules on the axle. In their initial state (i.e., not threaded), the cationic macrocycles experienced electrostatic repulsion with the axle molecules bearing cationic terminal ends. However, reducing the viologens on the axle and on the cyclic molecules allowed the latter to overcome the cationic terminals because the electrostatic repulsion between the cyclic molecules and terminal cations was reduced. Therefore, assembly on the reduced viologen station of the axle yielded threaded structure **23**. Further, subsequent oxidation decreased the affinity between the cyclic molecules and axle stations. Finally, because the resultant cationic macrocycles experienced electrostatic repulsion with the cationic terminals on the axle, the cyclic molecules moved to the central polymer chains (**24**) upon overcoming the steric bulk of the axle via heating. Hence, after one redox cycle, two cationic macrocycles were introduced onto the polymeric axle, providing poly[2*m* + 1]rotaxanes (**25**) through *m* redox cycles. The thus-formed polyrotaxane possessed multiple cationic macrocycles introduced using a molecular pumping technique. The systematic investigation of the effects of the cationic macrocycles revealed that increasing the number of cationic cycles increased the rigidity of the randomly coiled polymer chains as a result of the electrostatic repulsions between adjacent macrocycles. The precise molecular design and sequential redox reactions enabled the

number of cationic macrocycles in the polyrotaxane system to be defined. The critical strategy in this process is the selective tuning of the electrostatic interactions between macrocycles and axles through redox cycles, as well as the steric repulsion.

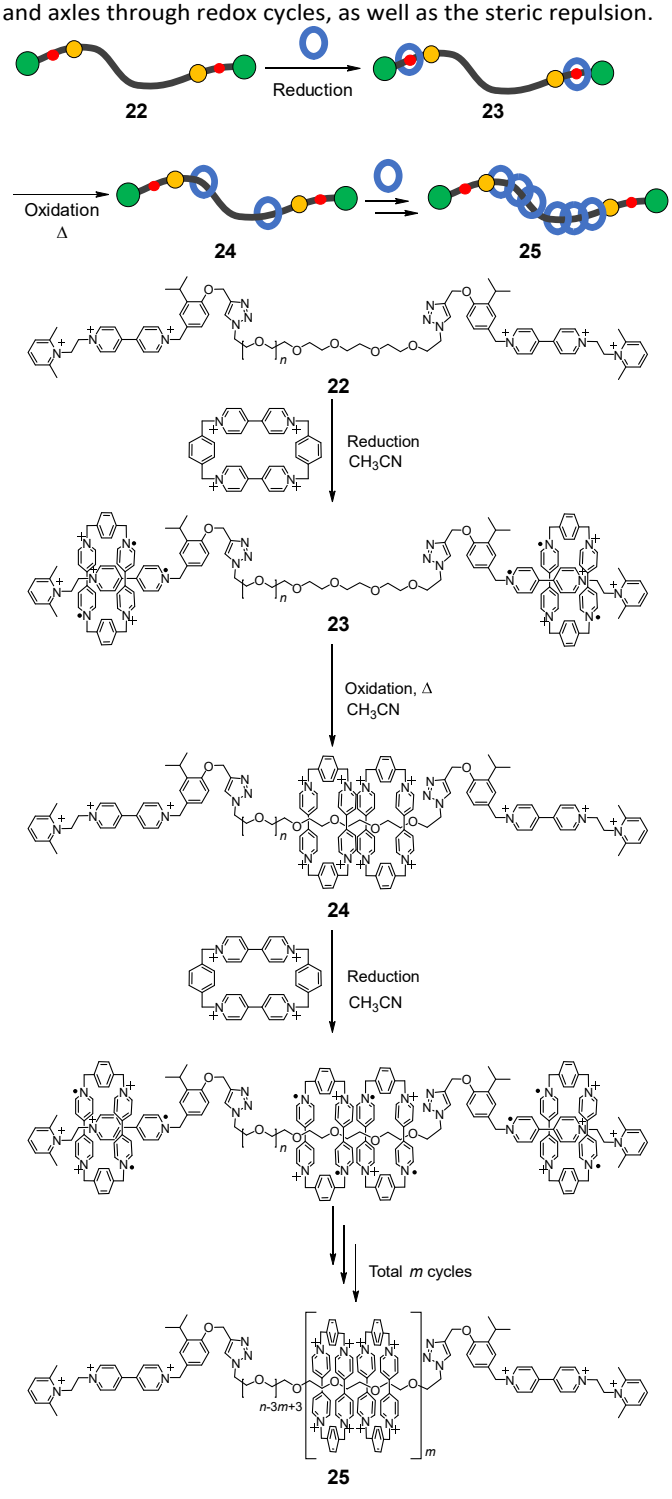

Fig. 9 Schematic representation and synthesis of poly[*n*]rotaxanes **25** via iterative redox cycles for cationic macrocycles and axles.[77]

4. Control of the positions of cyclic molecules

Recently, correlations between the functions of rotaxanes and the positions of the macrocycles on their axles have gained attention. In particular, the systematic investigation of these correlations would enable the design and development of functional rotaxane materials. One reasonable strategy to control the positions of macrocycles on an axle is to use block polymers as the rotaxane axles; this is because some macrocycles prefer a specific block polymer component, resulting in their localization. In 2019, Ito et al. reported the effects of the macrocyclic positions on the mechanical properties of polyrotaxanes.[78] They utilized a poly(ethylene oxide)-*b*-poly(propylene oxide)-*b*-poly(ethylene oxide) (PEO-PPO-PEO) triblock copolymer (**26**) as the axle backbone in the polyrotaxane system (Fig. 10a). Polyrotaxane **27** was synthesized via self-assembly between β-cyclodextrins (β-CDs) and the block-polymer, in which the β-CDs were localized on the PPO segments, followed by a capping reaction with bulky stopper units at both ends of the assembled axle.[79,80] The β-CDs on the polyrotaxane were chemically modified with a hydrophilic hydroxypropyl moiety to form **28**, followed by modification with a hydrophobic trimethyl silyl group to afford **29**. In the bulk material, **28** formed a melted state at high temperatures (Fig. 10b), and the hydrophilic β-CD derivatives became localized on the central PPO segments in the polyrotaxanes, thus forming self-assembled domains. In contrast, **29** formed an elastic state in the bulk material, even at high temperatures (Fig. 10c). Unlike **28**, the hydrophobic β-CD derivatives in **29** were localized on the PEO segments, and the self-assembled domains bridged each other to provide elasticity. This is rather like the supramolecular exchange of the block copolymer sequence, and resulted in bulk materials having mechanical properties governed by the positions of the macrocycles.

Flood et al. developed a supramolecular polymeric system based on electron-poor macrocycles (**30**) and diphosphate axles (**31**) (Fig. 11).[81,82] In this system, the phosphate-phosphate dimers were stabilized by two macrocycles via the formation of rotaxane structures as 2:2 complexes owing to the electrostatic interactions taking place.[83] The enhanced anion–anion bonding of the phosphate-phosphate dimers allowed supramolecular polymerization between the macrocycles and the diphosphate monomers. Moreover, the stoichiometric control between the macrocycles and the monomers (i.e., 1:1 ratio) provided an alternating copolymer (**32**) of threaded and non-threaded structures incorporating the acid dimers and two macrocycles. In contrast, a 2:1 stoichiometric ratio afforded a homopolymer (**33**) bearing only the rotaxane structures. Interestingly, homopolymer **33** possessed a stronger adhesion strength than copolymer **32**; this is because the electrostatic interactions between the two macrocycles located on the phosphate-phosphate dimers increased its degree of polymerization and adhesion strength, making them tunable by the stoichiometry.

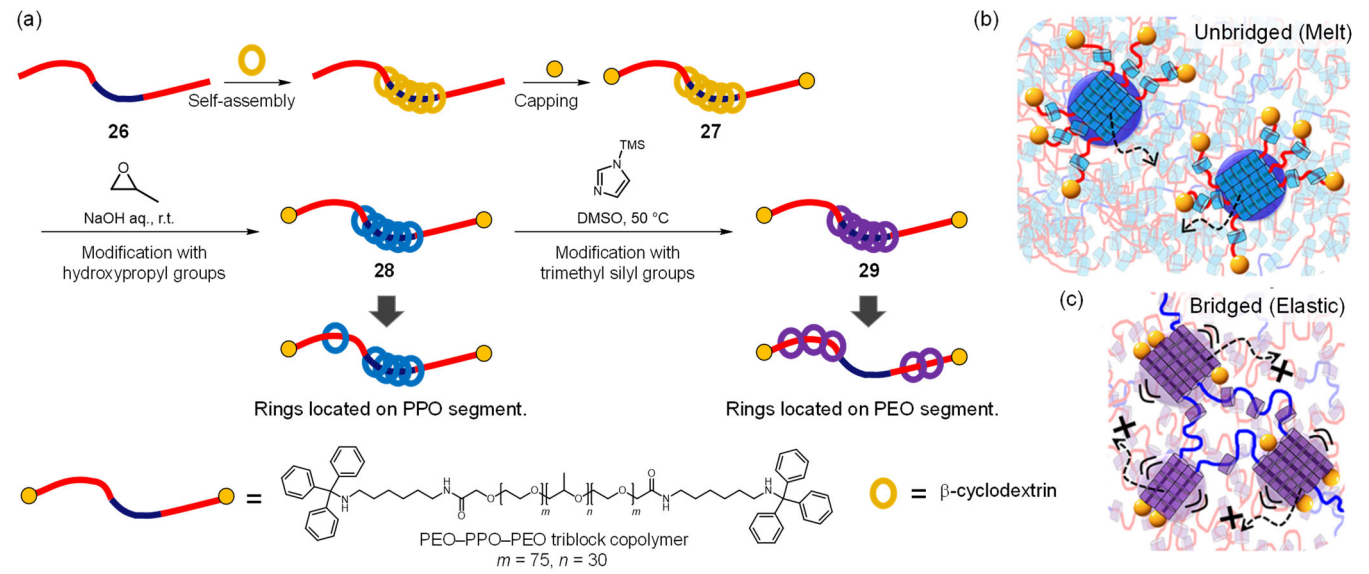

Fig. 10 (a) Synthesis of polyrotaxanes **28** and **29** bearing modified β-cyclodextrins with hydrophilic hydroxypropyl groups and hydrophobic trimethyl silyl groups, respectively, and conceptual illustrations of (b) **28** and (c) **29** in the bulk focusing on the self-assembled domains derived from the positions of the cyclic components on the axle.[78] Adapted with permission from Ref. 78. Copyright 2019 the American Chemical Society.

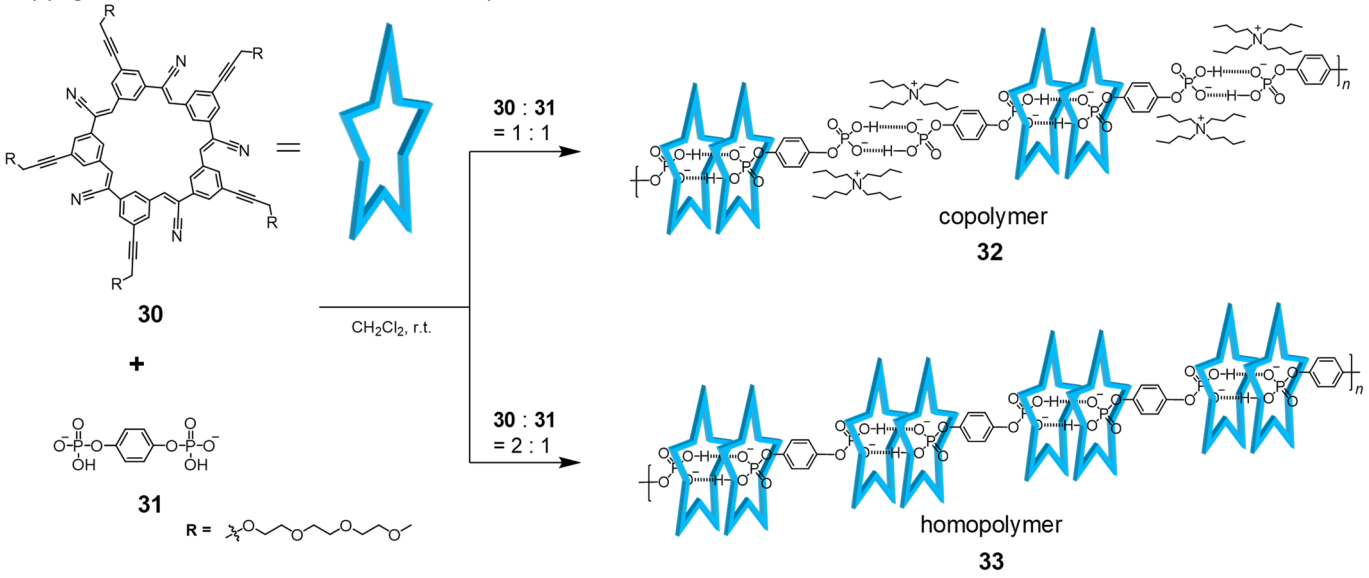

Fig. 11 Synthesis of supramolecular copolymer **32** and homopolymer **33**, tuned by the stoichiometry of the components.[82]

To define the positions of cyclic molecules on rotaxane axles, several strategies have been used. One strategy in early reports connected macrocycles to oligomer and polymer axle molecules via coordination bonds with copper(I) complexes, thus yielding oligo- and polyrotaxanes.[45–47,84,85] The coordination bonds prevented the dissociation of the macrocycles during oligomerization and polymerization and provided defined positions of the macrocycles on the axle. On the other hand, during the preparation of oligo- and polyrotaxanes, weak supramolecular interactions between the axle and the macrocycles can afford defects in the assembly, where some of the multiple macrocycles are not correctly incorporated onto the axle. One approach to prevent such defects includes increasing the binding constant between the axle and macrocycles. In general, the presence of multiple cavities in a host molecule results in a strong binding constant to the guest.[86] For example, Chen et al. developed a polyrotaxane synthesis based on a new type of host molecule, where two crown ether hosts were connected with a triptycene derivative.[87] The resulting pseudorotaxane (**34**) was stabilized by two binding moieties, wherein the axle molecule was associated with the host through two ammonium cations (Fig. 12a). The obtained pseudorotaxane was then polymerized via a

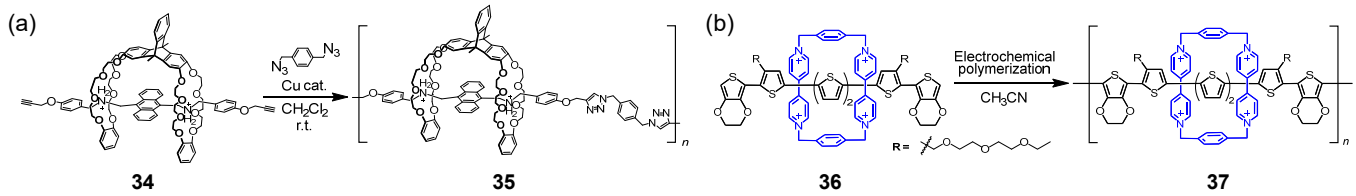

Fig. 12 (a) Synthesis of polyrotaxane **35** bearing multicavity macrocyclic host molecules.[87] (b) Synthesis of rotaxane-based polythiophene **37** via the polymerization of [2]rotaxane **36**. [89]

click reaction to provide polyrotaxane **35**. Another strategy defined the macrocycle positions in rotaxanes via oligomerization and polymerization of [2]rotaxanes bearing bulky stoppers at both ends.[88] Furthermore, Higuchi et al. developed a synthetic route employing the electrochemical reaction of [2]rotaxane-based oligothiophene **36** to give rotaxane-based polythiophene **37** (Fig. 12b).[89,90] Because of the stoppers, the dissociation of the macrocycles during polymerization was prevented, yielding a polyrotaxane system with no unthreaded repeating units, which are typically present as structural defects. The resultant polyrotaxanes possessed higher coverages than conventional polyrotaxanes, whose cyclic molecules typically dissociate during polymerization to produce defects on the polyrotaxane structure.[12,28]

This fixing strategy has been recently applied to using covalent linkages between rotaxane axle and cyclic molecules. So-called linked rotaxane structures ([1]rotaxanes)[91–93] have been prepared via polymerization with self-threading monomers, in which the axle units thread into the macrocyclic side chains.[94] The threading structures of [1]rotaxanes are maintained by covalent linkages instead of the bulky stoppers used with [2]rotaxanes (Fig. 13a). In addition, the cyclic components of [1]rotaxanes have fixed positions owing to these covalent linkages, whereas the macrocycles of conventional rotaxanes exhibit thermal shuttling. In particular, the [1]rotaxane strategy has enabled the formation of insulated conjugated polymers, which require a high macrocycle ratio on their π-conjugated polymer backbone. Specifically, because the macrocycles are covalently fixed on the axle monomers before polymerization, each repeating unit of the polymeric product is covered with defect-free insulating macrocycles; furthermore, the positions and number densities of the macrocycles on the axle are strictly defined by the covalent bonds. In 2006, Osuka et al. developed porphyrin polymers covered by cyclic alkyl chains bearing linked rotaxane structures (Fig. 13b).[95] Porphyrin polymers have attracted attention because of their electrical and optical properties.[96] The oxidative polymerization of porphyrin monomer **38** bearing self-threaded cyclic side chains provided linked-rotaxane-based porphyrin polymers **39** and **40**. These polymers were highly soluble because of their π-interactions were inhibited by the aliphatic macrocycles; meanwhile, conventional porphyrin polymers have strong π–π interactions, resulting in poor solubility.

In 2009, we reported a linked-rotaxane-based conjugated polymer bearing permethylated cyclodextrins (PM α-CDs). In this system, phenylene ethynylene monomers (**41**) having two PM α-CDs were covalently linked to a π-conjugated axle and then thermodynamically converted into self-inclusion complex

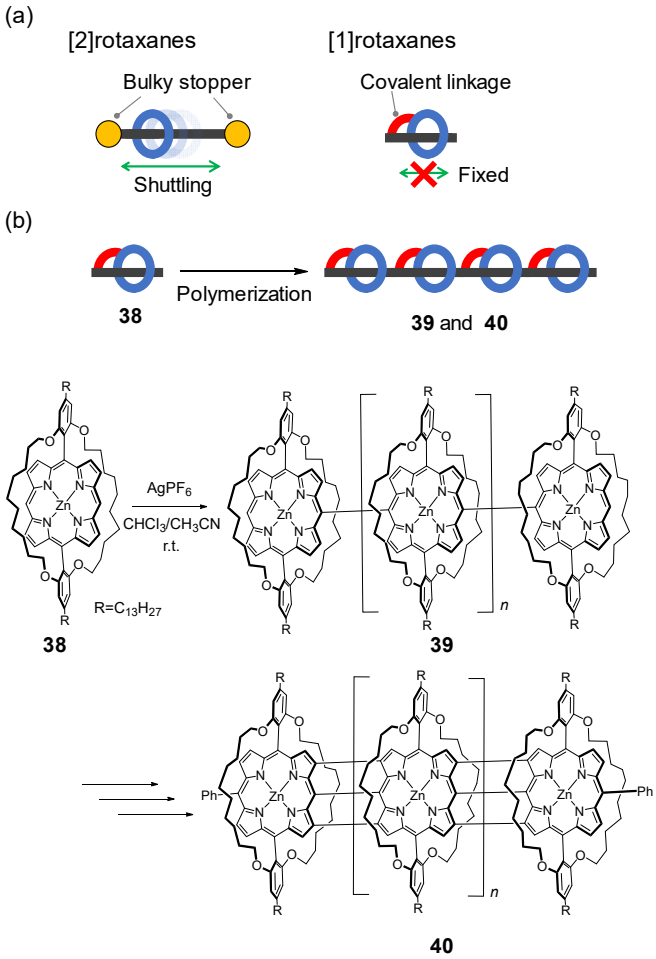

Fig. 13 (a) Schematic representations of [2]rotaxanes and [1]rotaxanes. (b) Schematic representation and synthesis of porphyrin polymers **39** and **40** bearing linked rotaxane structures.[95]

42 in high polarity solvents (MeOH/H_2O). At equilibrium, the Pd-catalyzed polymerization of **42** was conducted, which yielded insulated conjugated polymer **43** (Fig. 14a).[97,98] The resultant polymeric materials exhibited high intramolecular charge mobilities, even in the solid state, as determined by time-resolved microwave conductivity and transient absorption spectroscopy (TRMC-TAS) measurements;[99] this was because of the inhibited π–π interactions. Moreover, because of the high rigidity of the polymer backbone derived from the insulated structure, the insulated conjugated polymers exhibited high luminescence and liquid crystal behavior.[100,101] Moreover, we

also developed synthetic methods to simultaneously define the axle length and number of cyclic molecules to achieve an insulating layer on the linked rotaxane structures. The synthetic strategies employed iterative reactions based on Sonogashira coupling and terminal-alkyne deprotection reactions, and were conducted to elongate the [1]rotaxane backbone with the addition of two linked macrocycles in each step (Fig. 14b).[102] Moreover, by changing the solvent polarity, the supramolecular structure could be varied between insulated and uninsulated because of differences in thermodynamic stability. Specifically, carrying out the iterative reaction with a high polarity solvent (e.g., MeOH/H_2O) provided an elongated and insulated axle; whereas, when using a low polarity solvent (e.g., piperidine), an uninsulated axle was produced. The switching of solvent polarity in each iterative reaction enabled the synthesis of stereoisomers of [1]rotaxanes (**44** and **44'**) having defined axle lengths and positions of insulation on their axles; this was achievable because the cyclic molecules were covalently connected to the axle molecules, thus preventing shuttling. This strategy was also used to prepare linked [1]rotaxane **45** bearing 10 macrocycles on its axle, as well as a [1]rotaxane bearing non-centrosymmetric conjugated axle components.[103]

Macrocycles linked to the axle can also be utilized as light-harvesting moieties to improve the luminescence properties of these materials. Höger and Lupton et al. reported poly(phenylene ethynylene)-bearing conjugated macrocycles with covalent linkages to the axle polymer (Fig. 15).[104] A phenylene ethynylene monomer (**46**) connected to a π-conjugated ring with two ether bonds was polymerized via the oxidative coupling of the terminal alkynes. The resultant π-conjugated polymer (**47**) was encapsulated by π-conjugated rings, and the threaded structure of the conjugated polymer increased the rigidity of the π-conjugated backbone. In addition, the threaded polymer possessed a larger effective chain persistence length than the unthreaded polymer.[105] Moreover, light-harvesting was possible, and energy transfer from the conjugated rings to the conjugated polymers occurred upon excitation. Thus, these threaded structures composed of π-

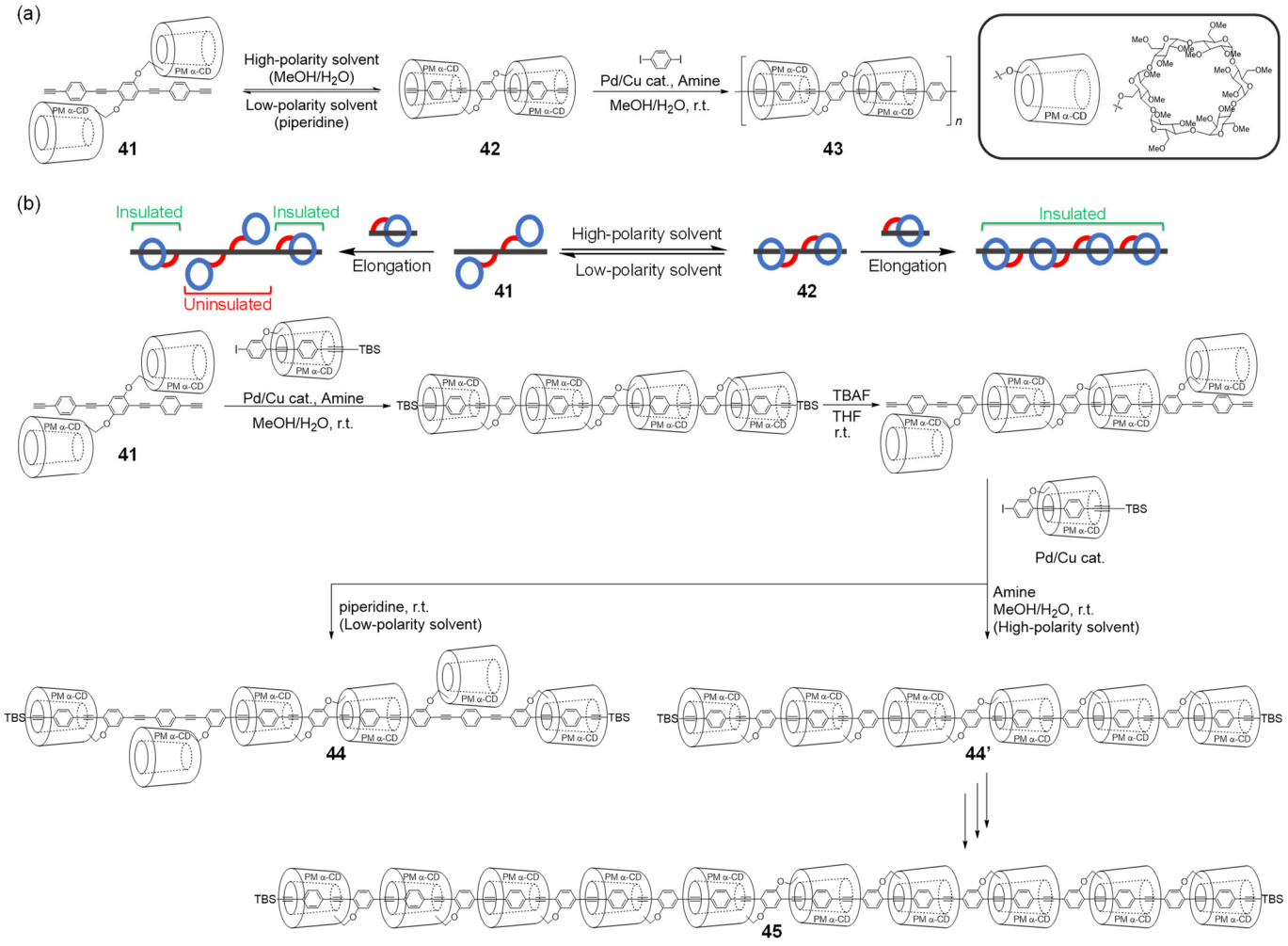

Fig. 14 (a) Syntheses of insulated conjugated polymers having phenylene ethynylene backbones bearing permethylated cyclodextrins (PM α-CDs) via the Pd-catalyzed polymerization of polymer **43**.[98] (b) Schematic representation and synthesis of the iterative reactions yielding stereoisomers **44** and **44'** having defined positions of their insulated regions, as well as [1]rotaxane **45** bearing 10 macrocycles on its axle.[102]

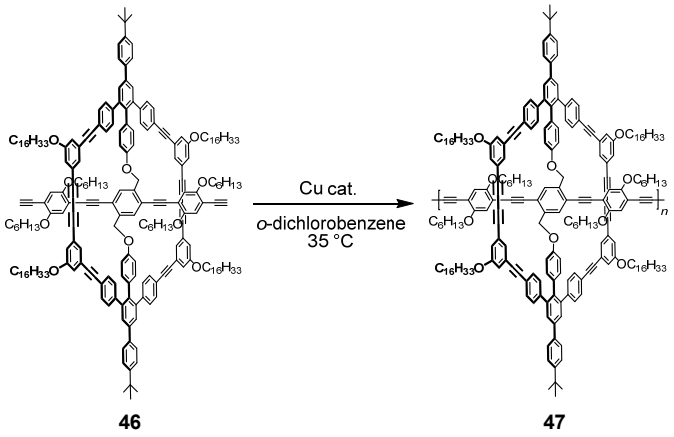

Fig. 15 Synthetic scheme of linked rotaxane polymer **47** with light-harvesting properties.[104]

conjugated axles and macrocycles could serve as energy-collecting systems.

Recently, linked rotaxanes have been used as precursors to prepare unlinked rotaxanes by cleavage of the covalent bonds between the axle and macrocycles (Fig. 16a).[106] These unlinked rotaxanes possess defined structures; specifically, defined number densities and sequences of macrocycles on their axles. For example, Grimme and Höger et al. preliminary synthesized a [1]rotaxane (**48**) composed of multiple linkages on each macrocycle: two rings at each end linked by stable ether bonds and a central ring linked by relatively weak ester bonds (Fig. 16b).[107] The sequence of the three macrocycles on the axle was determined using stepwise reactions, and the cleavage of the ester bonds was used to release the covalent bond connecting the central macrocycle to the axle, thus yielding a [2]rotaxane structure (**49**) bearing two linked rotaxane structures as bulky stoppers at both ends. Similarly, Maarseveen et al. carried out

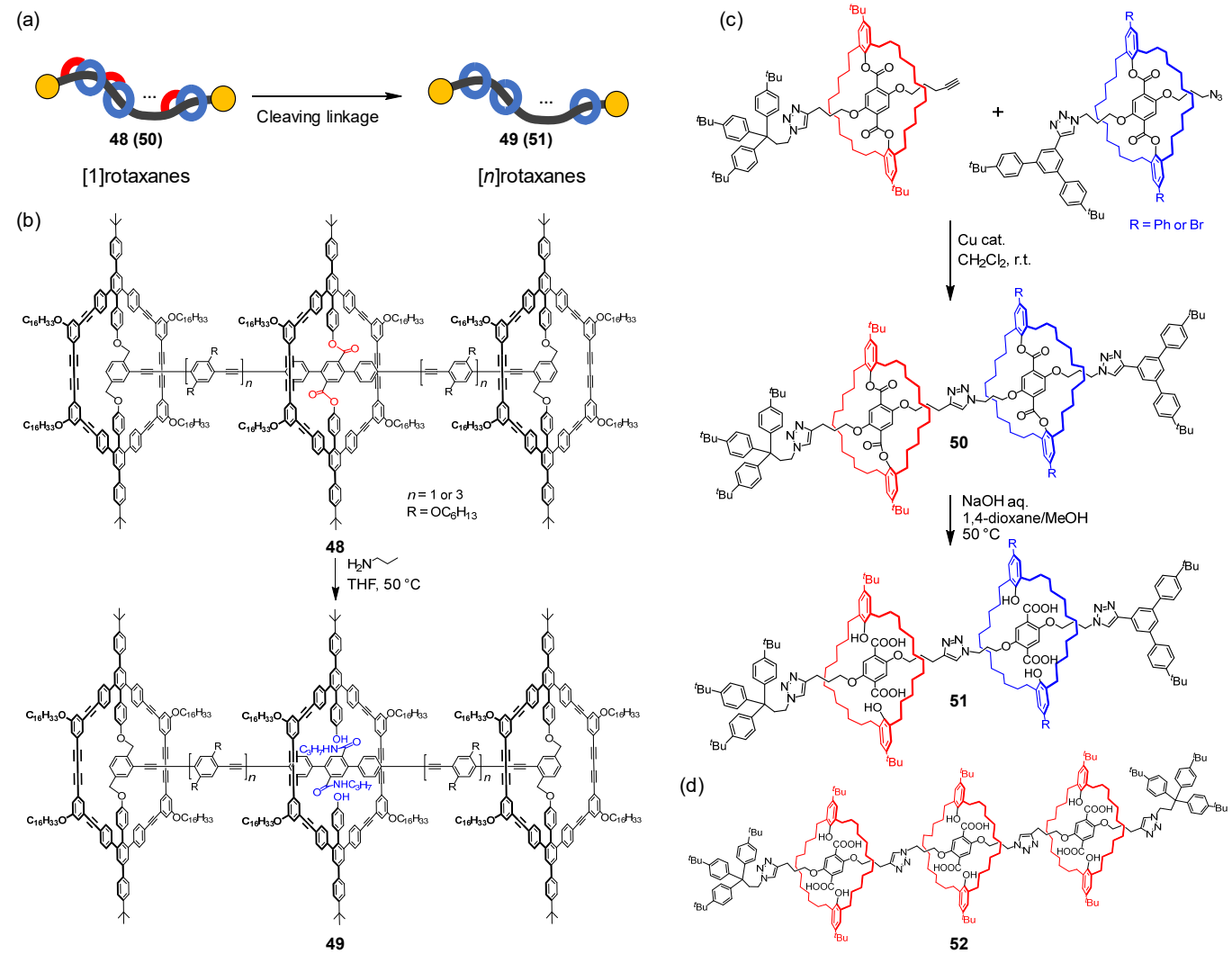

Fig. 16 (a) Schematic representation of [*n*]rotaxane syntheses proceeding via the cleavage of the covalent linkages in [1]rotaxanes. (b) Synthesis of [2]rotaxane **49** by cleaving the central linkage of [1]rotaxane **48**.[107] (c) Synthesis of structurally defined [3]rotaxane **51** via the hydrolysis of [1]rotaxane **50**. (d) Structure of [4]rotaxane **52**.[108]

the precision synthesis of a series of homo- and hetero[*n*]rotaxanes utilizing temporary covalent linkages (Figs. 16c and 16d).[108] They prepared [1]rotaxanes **50**, where two macrocycles and an axle were connected through ester bonds. This was achieved using Huisgen cycloadditions between the azido-terminated and ethynyl-terminated linked rotaxanes. The stepwise reactions afforded various types of [1]rotaxanes bearing diverse ring structures. Subsequently, the ester bonds were hydrolyzed to cleave the covalent linkages between the cyclic and axle components, providing [3]rotaxane **51** and [4]rotaxane **52** with defined ring numbers and components, even in the case of heterorotaxanes.

In 2010, Sugiyasu and Takeuchi et al. reported polythiophenes bearing self-threaded structure **55** via the polymerization of a precisely synthesized bithiophene moiety (**54**) bearing an alkyl cyclic unit as a side chain (Fig. 17a).[109] The aliphatic cyclic side chains inhibited the π–π interactions, and the insulated conjugated polymer (**55**) showed high intramolecular charge mobility, even in the solid state, as shown by TRMC-TAS measurements. In addition, co-polymerization between the self-threaded monomer and another monomer with various electron energy states provided solid-state fluorescent materials (**P1**–**P4**) exhibiting a wide range of luminescence colors, from purple to red (Figs. 17b and 17c).[110,111] The threaded structures enabled two polymers with different luminescence colors to be blended without microphase separation, where the blended polymer films displayed the sum of the luminescence colors of the components. Typically, blended π-conjugated polymers undergo microphase separation and energy transfer in the solid state as a result of strong π-interactions. The self-threading structures inhibited the π-interactions between chains because the polymer interactions were affected by the aliphatic macrocycles rather than the π-conjugation. The self-threading strategy was also applied to diketopyrrolopyrrole moieties (**56**) by Bronstein et al. (Fig. 17d).[112] A self-threaded monomer was copolymerized with a thiophene moiety to afford red luminescent materials in high quantum yields, even in the solid state. These results indicate that the self-threading strategy with defined structures is promising for various optical applications.

The precise engineering of the insulation position and coverage ratio of the axle of a threaded structure enables the effects of the structure on its insulating properties to be investigated. We have also evaluated the effects of the position of the insulated region to investigate ways to systematically enhance phosphorescence. To achieve this, we utilized linked rotaxanes with unmovable cyclic components to protect specific positions on the axle component, allowing us to identify the relationship between the insulation positions and phosphorescence enhancement (Fig. 18a).[113,114] Further, we synthesized various types of insulated conjugated polymers bearing Pt–acetylide complexes having different insulation positions and insulation densities (**57**–**60**). The observation of the phosphorescence revealed that the targeted insulation enhanced phosphorescence in both the solution and solid states by inhibiting the thermal fluctuations of the conjugated backbones; this was because the cyclic components improved the chain rigidity. Moreover, the perfect insulation of the conjugated backbone allowed phosphorescence in the solid state without quenching by intermolecular interactions. In addition, this insulation strategy was applied to produce color-tunable phosphorescent materials in the solid state using heteroaromatic Pt–acetylide complexes protected by PM α-CDs.[115]

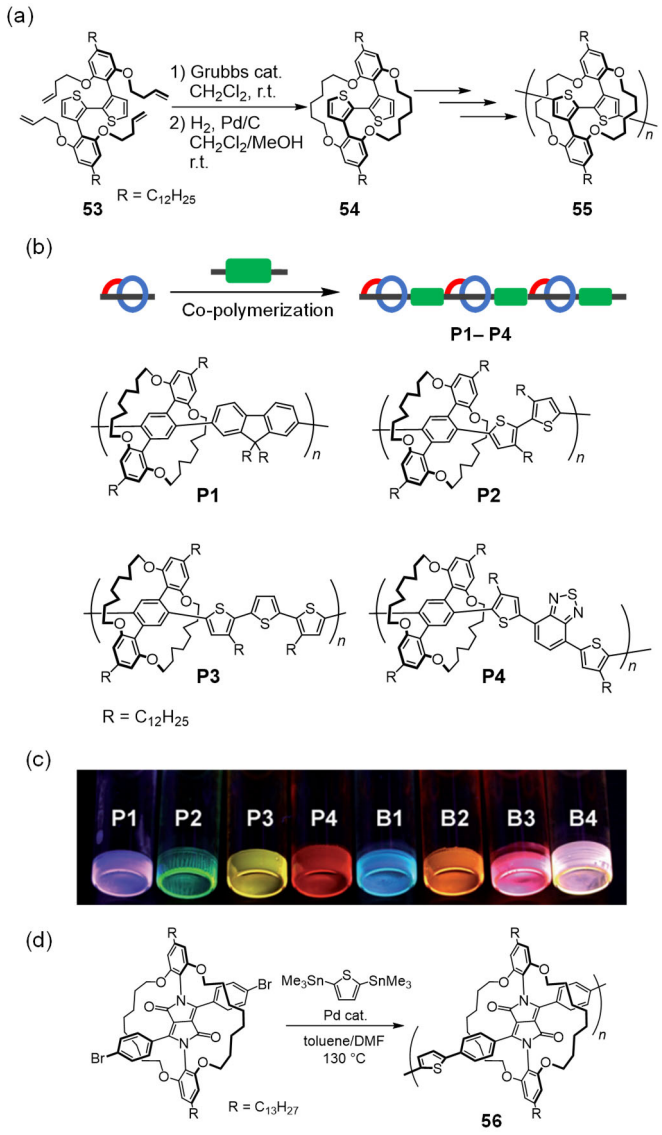

Fig. 17 (a) Synthetic scheme of insulated conjugated polymer **55** having a self-threaded structure.[109] (b) Schematic representation and structures of insulated co-polymers **P1**–**P4**. (c) Photographs of polymer films **P1**–**P4** and their blended films (**B1**–**B4**) under UV (365 nm) irradiation. Blending ratios: **B1** (**P1**/**P2** = 100/10), **B2** (**P3**/**P4** =100/5), **B3** (**P1**/**P4** = 100/5), and **B4** (**P1**/**P3**/**P4** = 200/3/1).[111] Adapted with permission from Ref. 111. Copyright 2013 Wiley-VCH Verlag GmbH & KaA, Weinheim. (d) Synthetic route to diketopyrrolopyrrole-based insulated conjugated polymer **56**.[112]

The systematic investigation of insulated polymers having linked rotaxane structures has enabled the enhancement in their electrical and optical properties. In one study, *para*-phenylene ethynylene units were used in the insulated backbone of such polymers, and the high rigidity of the conjugated backbones arising from the insulation resulted in improved conduction through the π-conjugated system. Moreover, the intramolecular charge mobility of the insulated *para*-phenylene ethynylene backbone (μ < 1 cm^2 V^{-1} s^{-1}) was further improved by the periodic introduction of *meta*-phenylene ethynylene moieties (Fig. 18b).[116] In more typical conjugated polymers, the conductive molecular orbitals are randomly twisted by thermal distortions and fluctuations, thus disconnects the delocalization and conductive properties. This thermally induced random loss of delocalization at ambient temperature remains a significant problem in the field of molecular devices. However, in conjugated systems bearing partial *meta*-connections, the molecular orbitals derived from the *para*-phenylene ethynylene moieties are periodically disconnected by the *meta*-phenylene ethynylene moieties (**61**–**63**). The localized conjugated system reduces these random disconnections, which increases intramolecular charge mobility through the conjugated backbones (up to μ = 8.5 cm^2 V^{-1} s^{-1}). However, the periodic *meta*-system showed lower conductivity than the ideal *para*-phenylene ethynylene conjugated structure, which does not suffer from thermal disconnection. Nevertheless, the periodic delocalization within the *meta*-system resulted in higher charge mobility at ambient temperature than that within the purely *para*-system. Thus, these results reveal a new design principle for the preparation of highly conductive organic materials for use under ambient conditions. These examples demonstrate that precisely

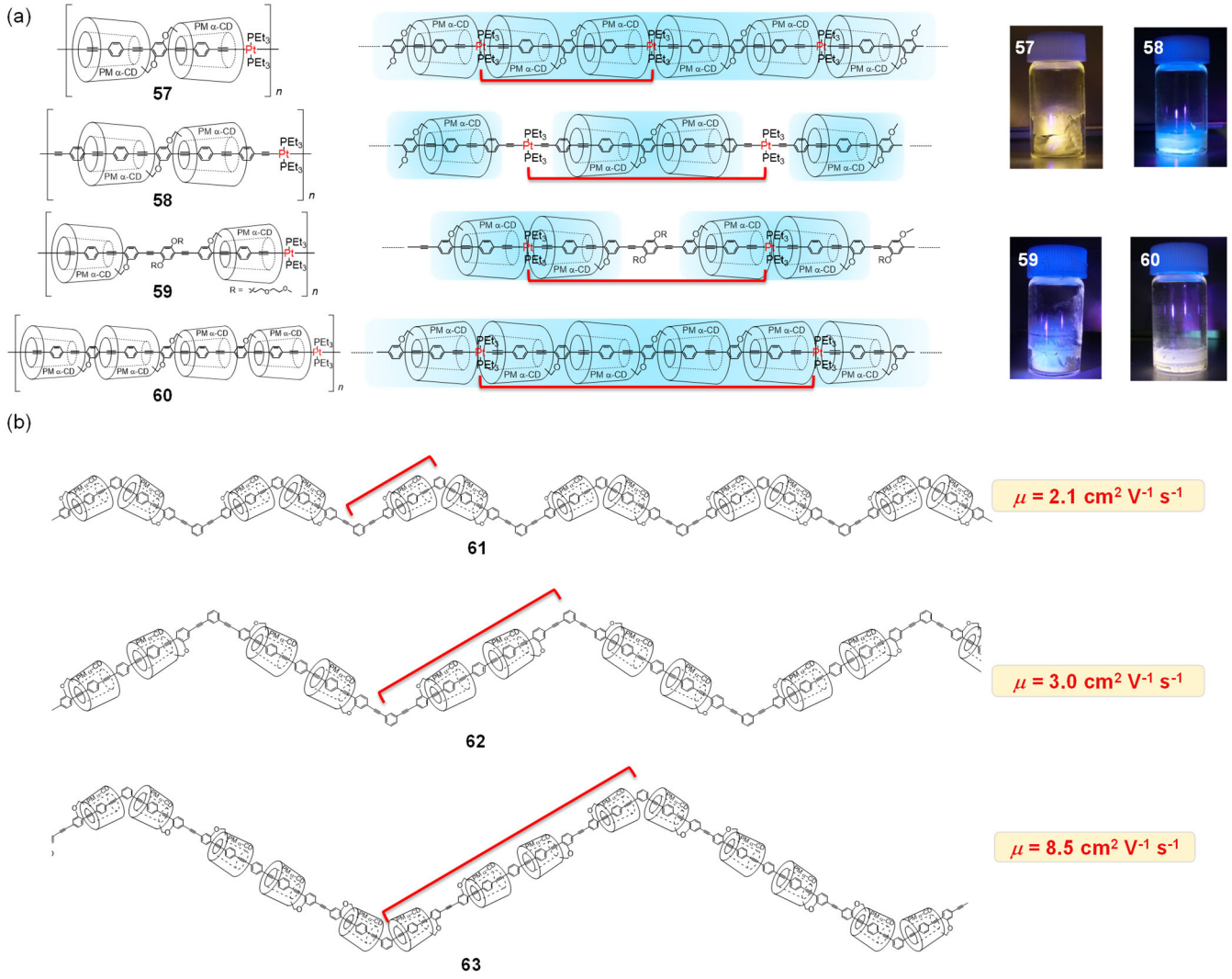

Fig. 18 (a) Chemical structures of Pt–acetylide-type insulated conjugated polymers **57**–**60** having different positions of insulation and different lengths of π-conjugated regions between their Pt-complexes. Photographs of these materials under UV (365 nm) light under deoxygenated conditions are also shown. In the chemical structures, the blue areas indicate the covalently fixed insulation areas and the red line denotes the conjugated backbones between Pt complexes.[114] Adapted with permission from Ref. 114. Copyright 2014 American Chemical Society. (b) Structures of insulated conjugated polymers **61**–**63** having periodic *meta*-junctions and their intramolecular charge mobilities.[116] The red lines indicate conjugation between periodic *meta*-junctions.

synthesized rotaxane structures having a defined number and position of macrocycles for insulation could be utilized as polymer components for advanced electronics and materials possessing excellent physical properties and functionalities.

In 2020, we reported an insulated conjugated metallopolymer showing unique responsiveness to CO gas concentration.[117] Two types of metal complexes containing Ru(II) and Pt(II) were connected by insulated π-conjugated backbones (Fig. 19a). The non-radiative insulated conjugated bimetallopolymer was depolymerized via ligand exchange reactions with CO gas at the Ru complex, affording a phosphorescent monomer containing a Pt complex. Overall, the profile of the emission intensity versus CO gas concentration after a certain reaction time was sigmoidal, having two threshold concentrations. At a low CO gas concentration (stage I), a few monomers were generated via the random depolymerization of polymers to oligomers, subsequently affording monomers over a certain concentration threshold. Accordingly, a combination of polymer-to-monomer conversion and monomer-induced output provided a threshold for activation in the chemical sensing reaction (stage II). In contrast, at higher concentrations of CO gas (stage III), the depolymerization reaction is constant because of the change in the rate-determining step in the ligand-exchange reaction of the Ru complex (dissociation or coordination).[118,119] The use of these two strategies within a single chemical compound afforded unprecedented artificial chemical sensors with biomimetic dual self-controlling responses.

Utilizing effective electronic communication through an insulated π-conjugated region, we have reported a luminescent metal-ion sensor based on a linked rotaxane structure (Fig. 19b).[120] Here, an ion-responsive moiety (2,2'-bipyridine) was introduced into the insulated conjugated polymer, which shows solid-state luminescence. As a result, the linked polyrotaxane (**64**) allows the sensing of typical metal ions via changes in its luminescence, even in the solid state. Crucially, the linked rotaxane structure prohibits the thermal sliding of the cyclic molecules on the axle. That is, the insulated, covalently linked structure selectively exposes the bipyridine unit to the outer environment, whereas the phenylene ethynylene moiety is protected. The well-defined insulated region on the axle enable both solid-state emission and the sensing of external stimuli. For example, changes in the luminescence color of a glass-plate coated with a film of the insulated polymer were observed after it was dipped into a Sn^{4+} solution and then an In^{3+} solution. The area showing a color change corresponded to the submerged area of the polymer film (Fig. 19c). Alongside sensing the presence of metal ions, the insulated polymer film selectively responds to the type of metal ion. Moreover, the initial color of the polymer films could be recovered after dipping into aqueous ammonia to release the metal ions from the bipyridine units. The coordination of the metal ions onto the bipyridine moieties affected the adjacent bipyridine units because of their

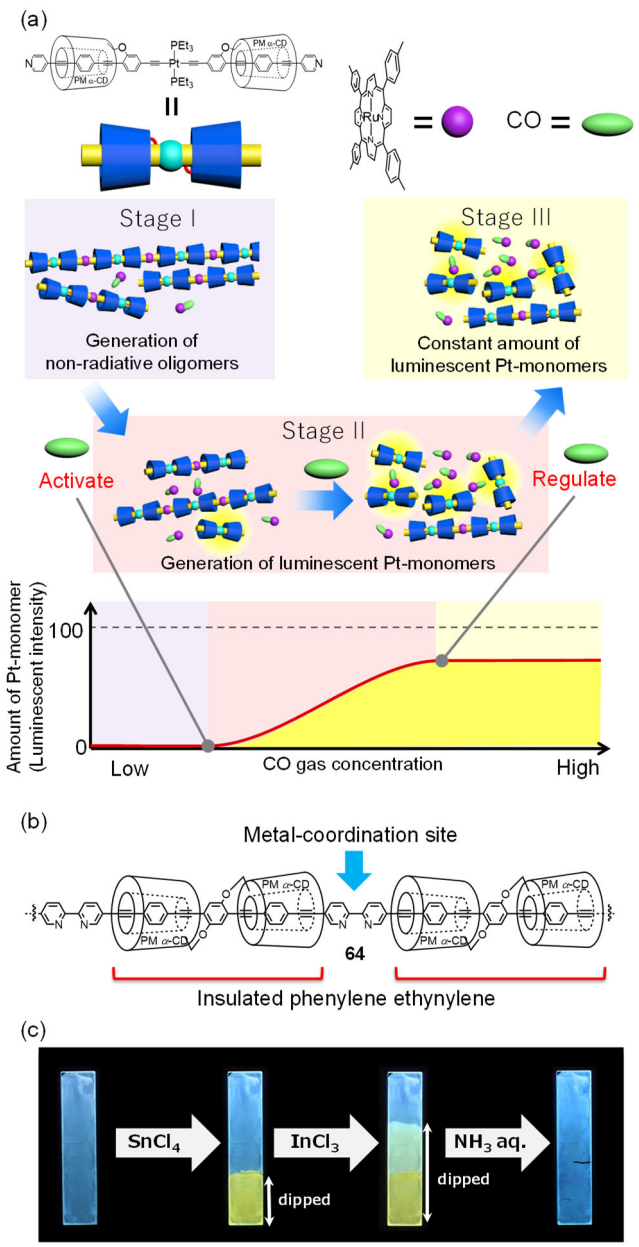

Fig. 19 (a) Conceptual representation of the sigmoidal response with two thresholds for changing the optical intensity with increasing CO gas concentration.[117] Adapted with permission from Ref. 117. Copyright 2020 Nature Publishing Group. (b) Structure of insulated polymer **64** having selectively insulated phenylene ethynylenes units and exposed bipyridine units as metal-coordination sites.[120] (c) Photograph (under 365 nm UV irradiation) of the reversible metal sensibility of a film of **64** on a SiO_2 substrate, achieved via sequential dipping into ion solutions ($SnCl_4$ and $InCl_3$ in Et_2O) and aqueous ammonia. Adapted with permission from Ref. 120. Copyright 2016 Wiley-VCH Verlag GmbH & KaA, Weinheim.

π-conjugation. As a result, the luminescence was quenched once approximately half of the bipyridine units had been coordinated by ions. Specifically, the ion-sensitivity of the material could be enhanced by utilizing effective energy transfer on the insulated π-conjugated polymer even in the solid state.

Conclusion and outlook

In summary, various reports have described the diverse synthetic methodologies and functions of oligorotaxanes and polyrotaxanes with precisely defined structures. In this context, the "defined" structural parameters include the numbers and positions of the macrocycles on the axles, which can be controlled using a range of synthetic protocols. The molecular weights and chemical structures of the axle and the cyclic components have been considered variable parameters. In addition, precise control of the structural parameters of the axle and the macrocycles is key to fine-tuning the functions of rotaxane-based materials. In the formative years of oligorotaxane synthesis, the addition of defined numbers of macrocycles onto an axle was achieved via sequential reactions during the preparation of the axle molecules, or through the self-assembly of the macrocycles. Recently, diverse strategies have been developed to define the numbers and positions of cyclic molecules on oligorotaxane and polyrotaxane axles. The developed strategies have provided unconventional rotaxanes, including supramolecular stereoisomers, via selective synthetic methods or out-of-equilibrium species based on molecular pumps. In addition, the precise and systematic synthesis of oligo- and polyrotaxanes has revealed that the position, number, and type of cyclic components in the rotaxanes are critical factors for governing the physical properties, similar to the conventional parameters including polydispersity indices, monomer sequences, and tacticities of polymeric materials.

In such carefully designed rotaxane systems, the number density of the cyclic components influences the shuttling effects on the axle. More specifically, rotaxanes with small numbers of macrocycles provide highly effective shuttling, which ultimately improves the toughness of the polyrotaxane network materials. In contrast, rotaxanes with large numbers of macrocycles can exhibit a reduced shuttling effect owing to steric repulsion, although the protecting effects of the axle could be enhanced, especially in the case of insulated conjugated polymers. However, the incorporation of such large numbers of cyclic components is difficult via typical rotaxane synthetic strategies, and tends to result in defects related to the macrocycles present on the axle. Covalently linked rotaxanes ([1]rotaxanes) have therefore been developed for the synthesis of highly insulated rotaxane structures, and such systems are known to exhibit unique optical and electrical functionalities. Moreover, recent studies have constructed out-of-equilibrium polyrotaxanes via a molecular pump strategy, where the highly densified macrocycles rigidify the polymer axle owing to their electrostatic repulsive forces.

In terms of the positions of the cyclic components on the axle, an increasing number of studies have revealed the importance of this factor in determining the properties of oligorotaxane and polyrotaxane materials. For example, recent research clarified that the positions of the cyclic molecules of these materials affects their elasticities. Conventionally, for a small number of cyclic components (e.g., [2]rotaxane), the positions of the macrocycles have been controlled via stimuli-responsive shuttling to provide molecular switches and machines. However, it remains a challenge to accurately define each macrocyclic position in rotaxanes containing large numbers of cyclic components. Linked rotaxanes ([1]rotaxanes) are considered a promising approach to address this issue, as the numbers and positions of their cyclic components can be tuned. In this context, it should be noted that systematic comparisons of various [1]rotaxanes bearing their cyclic components at different positions have clarified the effects of these structural parameters on the rotaxane properties, including variations in their optical and electrical properties derived from their insulation.

Recent studies have also shown that the sequence of the cyclic components on the rotaxane axle could be controlled via strategies such as self-sorting, iterative reactions, or the conversion of [1]rotaxanes to [*n*]rotaxanes. However, to date, the examples of sequence-controlled oligorotaxanes and polyrotaxanes in materials synthesis are limited. Moreover, it is expected that supramolecular stereoisomers could help to reveal the effects of multiple cyclic components on the material properties of rotaxane-based systems.

Accordingly, the precise syntheses of oligorotaxanes and polyrotaxanes have enabled the systematic investigation and clarification of the relationships between the threading parameters and properties of these unique materials, which will ultimately enable higher-order control over the physical properties and functions of such macromolecular materials. As mentioned in this *Feature Article*, oligo- and polyrotaxanes with well-defined structural parameters hold enormous potential for discovering unprecedented properties of rotaxane materials and for revealing their optimal molecular designs. However, progress in this area currently relies on two aspects, namely the development of the synthetic strategies toward such fine structures, and the appropriate and systematic evaluation of their material properties. Indeed, recent studies have gradually uncovered the relationships between the structural parameters and material properties of rotaxanes, but only a limited number of systems have been examined. Future research efforts into the precise synthesis of the rotaxane system should ideally focus on diversifying the fundamental strategies for constructing these systems, and their applications in the various fields of materials science.

Conflicts of interest

There are no conflicts to declare.

Acknowledgements

The authors would appreciate financial supports (JSPS Research Fellow, JSPS KAKENHI Grant Numbers 19H02696, 20H05092, 20H02159, 21K05181, and 21H00018, JST CREST Grant Number JPMJCR19I2, "Innovation inspired by Nature" Research Support Program, SEKISUI CHEMICAL CO., LTD., Takahashi Industrial and Economic Research Foundation TEPCO Memorial Foundation, The Sumitomo Foundation, Kumagai Foundation, and Inamori Foundation).

Notes and references

1 C. J. Bruns and J. F. Stoddart, *The Nature of the Mechanical Bond:From Molecules to Machines*, Wiley, 2016.

2 J. E. M. Lewis, M. Galli and S. M. Goldup, *Chem. Commun.*, 2017, **53**, 298–312.

3 K. M. Bąk, K. Porfyrakis, J. J. Davis and P. D. Beer, *Mater. Chem. Front.*, 2020, **4**, 1052–1073.

4 A. Martinez-Cuezva, A. Saura-Sanmartin, M. Alajarin and J. Berna, *ACS Catal.*, 2020, **10**, 7719–7733.

5 B. Taghavi Shahraki, S. Maghsoudi, Y. Fatahi, N. Rabiee, S. Bahadorikhalili, R. Dinarvand, M. Bagherzadeh and F. Verpoort, *Coord. Chem. Rev.*, 2020, **423**, 213484.

6 P. Waelès, M. Gauthier and F. Coutrot, *Angew. Chem., Int. Ed.*, 2021, **60**, 2–24.

7 M. Xue, Y. Yang, X. Chi, X. Yan and F. Huang, *Chem. Rev.*, 2015, **115**, 7398–7501.

8 S. Erbas-Cakmak, D. A. Leigh, C. T. McTernan and A. L. Nussbaumer, *Chem. Rev.*, 2015, **115**, 10081–10206.

9 S. Kassem, T. Van Leeuwen, A. S. Lubbe, M. R. Wilson, B. L. Feringa and D. A. Leigh, *Chem. Soc. Rev.*, 2017, **46**, 2592–2621.

10 A. Harada, A. Hashidzume, H. Yamaguchi and Y. Takashima, *Chem. Rev.*, 2009, **109**, 5974–6023.

11 Y. Kobayashi, *Polym. J.*, 2021, **53**, 505–513.

12 A. Harada, J. Li and M. Kamachi, *Nature*, 1992, **356**, 325–327.

13 A. Harada, J. Li and M. Kamachi, *Nature*, 1993, **364**, 516–518.

14 A. Harada, J. Li and M. Kamachi, *Nature*, 1994, **370**, 126–128.

15 A. Harada, J. Li and M. Kamachi, *J. Am. Chem. Soc.*, 1994, **116**, 3192–3196.

16 H. W. Gibson and H. Marand, *Adv. Mater.*, 1993, **5**, 11–21.

17 D. Tuncel and J. H. G. Steinke, *Chem. Commun.*, 1999, 1509–1510.

18 T. Ogoshi, Y. Nishida, T. A. Yamagishi and Y. Nakamoto, *Macromolecules*, 2010, **43**, 7068–7072.

19 N. Momčilović, P. G. Clark, A. J. Boydston and R. H. Grubbs, *J. Am. Chem. Soc.*, 2011, **133**, 19087–19089.

20 L. Fang, M. A. Olson, D. Benítez, E. Tkatchouk, W. A. Goddard and J. F. Stoddart, *Chem. Soc. Rev.*, 2010, **39**, 17–29.

21 M. Arunachalam and H. W. Gibson, *Prog. Polym. Sci.*, 2014, **39**, 1043–1073.

22 N. Hoyas Pérez and J. E. M. Lewis, *Org. Biomol. Chem.*, 2020, **18**, 6757–6780.

23 K. Yang, S. Chao, F. Zhang, Y. Pei and Z. Pei, *Chem. Commun.*, 2019, **55**, 13198–13210.

24 Y. Okumura and K. Ito, *Adv. Mater.*, 2001, **13**, 485–487.

25 A. Bin Imran, K. Esaki, H. Gotoh, T. Seki, K. Ito, Y. Sakai and Y. Takeoka, *Nat. Commun.*, 2014, **5**, 5124.

26 C. Liu, N. Morimoto, L. Jiang, S. Kawahara, T. Noritomi, H. Yokoyama, K. Mayumi and K. Ito, *Science*, 2021, **372**, 1078–1081.

27 F. Cacialli, J. S. Wilson, J. J. Michels, C. Daniel, C. Silva, R. H. Friend, N. Severin, P. Samorì, J. P. Rabe, M. J. O'Connell, P. N. Taylor and H. L. Anderson, *Nat. Mater.*, 2002, **1**, 160–164.

28 M. J. Frampton and H. L. Anderson, *Angew. Chem., Int. Ed.*, 2007, **46**, 1028–1064.

29 J. Royakkers and H. Bronstein, *Macromolecules*, 2021, **54**, 1083–1094.

30 S. Mena-Hernando and E. M. Pérez, *Chem. Soc. Rev.*, 2019, **48**, 5016–5032.

31 L. F. Hart, J. E. Hertzog, P. M. Rauscher, B. W. Rawe, M. M. Tranquilli and S. J. Rowan, *Nat. Rev. Mater.*, 2021, **6**, 508–530.

32 L. Jiang, C. Liu, K. Mayumi, K. Kato, H. Yokoyama and K. Ito, *Chem. Mater.*, 2018, **30**, 5013–5019.

33 K. Kato, Y. Okabe, Y. Okazumi and K. Ito, *Chem. Commun.*, 2015, **51**, 16180–16183.

34 J.-F. Lutz, M. Ouchi, D. R. Liu and M. Sawamoto, *Science*, 2013, **341**, 1238149.

35 M. Ouchi, T. Terashima and M. Sawamoto, *Chem. Rev.*, 2009, **109**, 4963–5050.

36 J. C. Worch, H. Prydderch, S. Jimaja, P. Bexis, M. L. Becker and A. P. Dove, *Nat. Rev. Chem.*, 2019, **3**, 514–535.

37 G. Agam, D. Graiver and A. Zilkha, *J. Am. Chem. Soc.*, 1976, **98**, 5206–5214.

38 I. T. Harrison and S. Harrison, *J. Am. Chem. Soc.*, 1967, **89**, 5723–5724.

39 J. E. Beves, B. A. Blight, C. J. Campbell, D. A. Leigh and R. T. McBurney, *Angew. Chem., Int. Ed.*, 2011, **50**, 9260–9327.

40 G. Barin, A. Coskun, M. M. G. Fouda and J. F. Stoddart, *Chempluschem*, 2012, **77**, 159–185.

41 N. H. Evans, *Eur. J. Org. Chem.*, **21**, 2019, 3320–3343.

42 H. -Y. Zhou, Q. -S. Zong, Y. Han and C. -F. Chen, *Chem. Commun.*, 2020, **56**, 9916–9936.

43 Here, the typical nomenclature for classifying rotaxane structures is introduced, i.e., [*n*]rotaxanes, where *n* is a sum number of the components of the rotaxane, that is, the total number of the axle molecules and cyclic molecules.

44 Z. He, W. Jiang and C. A. Schalley, *Chem. Soc. Rev.*, 2015, **44**, 779–789.

45 N. Solladié, J.-C. Chambron, C. O. Dietrich-Buchecker and J.-P. Sauvage, *Angew. Chem., Int. Ed.*, 1996, **35**, 906–909.

46 N. Solladié, J. Chambron and J. -P. Sauvage, *J. Am. Chem. Soc.*, 1999, **121**, 3684–3692.

47 J. P. Collin, S. Durot, M. Keller, J. P. Sauvage, Y. Trolez, M. Cetina and K. Rissanen, *Chem. -Eur. J.*, 2011, **17**, 947–957.

48 P. R. Ashton, R. Ballardini, V. Balzani, M. Bělohradský, M. T. Gandolfi, D. Philp, L. Prodi, F. M. Raymo, M. V Reddington, N. Spencer, J. F. Stoddart, M. Venturi and D. J. Williams, *J. Am. Chem. Soc.*, 1996, **118**, 4931–4951.

49 J. Wu, K. C.-F. Leung and J. F. Stoddart, *Proc. Natl. Acad. Sci. U. S. A.*, 2007, **104**, 17266–17271.

50 M. E. Belowich, C. Valente, R. A. Smaldone, D. C. Friedman, J. Thiel, L. Cronin and J. F. Stoddart, *J. Am. Chem. Soc.*, 2012, **134**, 5243–5261.

51 W. Zhang, W. R. Dichtel, A. Z. Stieg, D. Benítez, J. K. Gimzewski, J. R. Heath and J. F. Stoddart, *Proc. Natl. Acad. Sci. U. S. A.*, 2008, **105**, 6514–6519.
52 Z. Zhu, C. J. Bruns, H. Li, J. Lei, C. Ke, Z. Liu, S. Shafaie, H. M. Colquhoun and J. F. Stoddart, *Chem. Sci.*, 2013, **4**, 1470–1483.
53 D. Sluysmans, S. Hubert, C. J. Bruns, Z. Zhu, J. F. Stoddart and A. -S. Duwez, *Nat. Nanotechnol.*, 2018, **13**, 209–213.
54 D. Sluysmans, F. Devaux, C. J. Bruns, J. F. Stoddart and A. -S. Duwez, *Proc. Natl. Acad. Sci. U. S. A.*, 2018, **115**, 9362–9366.
55 W. Jiang, H. D. F. Winkler and C. A. Schalley, *J. Am. Chem. Soc.*, 2008, **130**, 13852–13853.
56 C. Ke, R. A. Smaldone, T. Kikuchi, H. Li, A. P. Davis and J. F. Stoddart, *Angew. Chem., Int. Ed.*, 2013, **52**, 381–387.
57 E. A. Neal and S. M. Goldup, *Angew. Chem., Int. Ed.*, 2016, **55**, 12488–12493.
58 Z. -J. Zhang, H. -Y. Zhang, H. Wang and Y. Liu, *Angew. Chem., Int. Ed.*, 2011, **50**, 10834–10838.
59 S. -J. Rao, Q. Zhang, J. Mei, X. -H. Ye, C. Gao, Q. -C. Wang, D. -H. Qu and H. Tian, *Chem. Sci.*, 2017, **8**, 6777–6783.
60 P. R. Ashton, P. T. Glink, M. V. Martínez-Díaz, J. F. Stoddart, A. J. P. White and D. J. Williams, *Angew. Chem., Int. Ed.*, 1996, **35**, 1930–1933.
61 H. Noguchi, K. Hojo and M. Suginome, *J. Am. Chem. Soc.*, 2007, **129**, 758–759.
62 E. P. Gillis and M. D. Burke, *J. Am. Chem. Soc.*, 2007, **129**, 6716–6717.
63 R. K. Roy, A. Meszynska, C. Laure, L. Charles, C. Verchin and J.-F. Lutz, *Nat. Commun.*, 2015, **6**, 7237.
64 J. C. Barnes, D. J. C. Ehrlich, A. X. Gao, F. A. Leibfarth, Y. Jiang, E. Zhou, T. F. Jamison and J. A. Johnson, *Nat. Chem.*, 2015, **7**, 810-815.
65 M. Porel and C. A. Alabi, *J. Am. Chem. Soc.*, 2014, **136**, 13162–13165.
66 A. H. Parham, R. Schmieder and F. Vögtle, *Synlett*, 1999, **12**, 1887–1890.
67 M. Radha Kishan, A. Parham, F. Schelhase, A. Yoneva, G. Silva, X. Chen, Y. Okamoto and F. Vögtle, *Angew. Chem., Int. Ed.*, 2006, **45**, 7296–7299.
68 A. M. L. Fuller, D. A. Leigh and P. J. Lusby, *Angew. Chem., Int. Ed.*, 2007, **46**, 5015–5019.
69 A. M. L. Fuller, D. A. Leigh and P. J. Lusby, *J. Am. Chem. Soc.*, 2010, **132**, 4954–4959.
70 J. E. M. Lewis, J. Winn, L. Cera and S. M. Goldup, *J. Am. Chem. Soc.*, 2016, **138**, 16329–16336.
71 J. D. Crowley, S. M. Goldup, A. -L. Lee, D. A. Leigh and R. T. Mc Burney, *Chem. Soc. Rev.*, 2009, **38**, 1530–1541.
72 S. Erbas-Cakmak, S. D. P. Fielden, U. Karaca, D. A. Leigh, C. T. McTernan, D. J. Tetlow and M. R. Wilson, *Science*, 2017, **358**, 340–343.
73 R. D. Astumian, C. Pezzato, Y. Feng, Y. Qiu, P. R. McGonigal, C. Cheng and J. F. Stoddart, *Mater. Chem. Front.*, 2020, **4**, 1304–1314.
74 S. Amano, S. D. P. Fielden and D. A. Leigh, *Nature*, 2021, **594**, 529–534.
75 C. Tian, S. D. P. Fielden, G. F. S. Whitehead, I. J. Vitorica-Yrezabal and D. A. Leigh, *Nat. Commun.*, 2020, **11**, 744.
76 S. A. P. van Rossum, M. Tena-Solsona, J. H. van Esch, R. Eelkema and J. Boekhoven, *Chem. Soc. Rev.*, 2017, **46**, 5519–5535.
77 Y. Qiu, B. Song, C. Pezzato, D. Shen, W. Liu, L. Zhang, Y. Feng, Q. H. Guo, K. Cai, W. Li, H. Chen, M. T. Nguyen, Y. Shi, C. Cheng, R. D. Astumian, X. Li and J. F. Stoddart, *Science*, 2020, **368**, 1247–1253.
78 S. Uenuma, R. Maeda, K. Kato, K. Mayumi, H. Yokoyama and K. Ito, *ACS Macro Lett.*, 2019, **8**, 140–144.
79 C. -C. Tsai, S. Leng, K. -U. Jeong, R. M. van Horn, C. -L. Wang, W. -B. Zhang, M. J. Graham, J. Huang, R. -M. Ho, Y. Chen, B. Lotz and S. Z. D. Cheng, *Macromolecules*, 2010, **43**, 9454–9461.
80 S. Uenuma, R. Maeda, S. Takahashi, K. Kato, H. Yokoyama and K. Ito, *Chem. Lett.*, 2016, **45**, 991–993.
81 W. Zhao, B. Qiao, J. Tropp, M. Pink, J. D. Azoulay and A. H. Flood, *J. Am. Chem. Soc.*, 2019, **141**, 4980–4989.
82 W. Zhao, J. Tropp, B. Qiao, M. Pink, J. D. Azoulay and A. H. Flood, *J. Am. Chem. Soc.*, 2020, **142**, 2579–2591.
83 E. M. Fatila, E. B. Twum, A. Sengupta, M. Pink, J. A. Karty, K. Raghavachari and A. H. Flood, *Angew. Chem., Int. Ed.*, 2016, **55**, 14057–14062.
84 S. S. Zhu, P. J. Carroll and T. M. Swager, *J. Am. Chem. Soc.*, 1996, **118**, 8713–8714.
85 S. S. Zhu and T. M. Swager, *J. Am. Chem. Soc.*, 1997, **119**, 12568–12577.
86 W. -B. Hu, W. -J. Hu, Y. A. Liu, J. -S. Li, B. Jiang and K. Wen, *Chem. Commun.*, 2016, **52**, 12130–12142.
87 F. Zeng, Z. Meng, Y. Han and C. -F. Chen, *Chem. Commun.*, 2014, **50**, 7611–7613.
88 T. J. Kidd, T. J. A. Loontjens, D. A. Leigh and J. K. Y. Wong, *Angew. Chem., Int. Ed.*, 2003, **42**, 3379–3383.
89 T. Ikeda, M. Higuchi and D. G. Kurth, *J. Am. Chem. Soc.*, 2009, **131**, 9158–9159.
90 T. Ikeda and M. Higuchi, *Langmuir*, 2011, **27**, 4184–4189.
91 R. Jäger, M. Händel, J. Harren, F. Vögtle and K. Rissanen, *L iebigs Ann. chem.*, 1996, 1201–1207.
92 C. Reuter, A. Mohry, A. Sobanski and F. Vögtle, *Chem. -Eur. J.*, 2000, **6**, 1674–1682.
93 O. Safarowsky, B. Windisch, A. Mohry and F. Vögtle, *J. Prakt. Chem.*, 2000, **342**, 437–444.
94 C. Pan, C. Zhao, M. Takeuchi and K. Sugiyasu, *Chem. Asian J.*, 2015, **10**, 1820–1835.
95 T. Ikeda, J. M. Lintuluoto, N. Aratani, Z. S. Yoon, D. Kim and A. Osuka, *Eur. J. Org. Chem.*, 2006, 3193–3204.
96 T. Tanaka and A. Osuka, *Chem. Soc. Rev.*, 2015, **44**, 943–969.
97 J. Terao, S. Tsuda, Y. Tanaka, K. Okoshi, T. Fujihara, Y. Tsuji and N. Kambe, *J. Am. Chem. Soc.*, 2009, **131**, 16004–16005.
98 J. Terao, Y. Tanaka, S. Tsuda, N. Kambe, M. Taniguchi, T. Kawai, A. Saeki and S. Seki, *J. Am. Chem. Soc.*, 2009, **131**, 18046–18047.
99 A. Saeki, Y. Koizumi, T. Aida and S. Seki, *Acc. Chem. Res.*, 2012, **45**, 1193–1202.
100 H. Masai and J. Terao, *Bull. Chem. Soc. Jpn.*, 2019, **92**, 529–539.
101 H. Masai and J. Terao, *Polym. J.*, 2017, **49**, 805–814.

102 H. Masai, T. Fujihara, Y. Tsuji and J. Terao, *Chem. -Eur. J.*, 2017, **23**, 15073–15079.
103 S. -Y. Chou, H. Masai, S. Tsuda and J. Terao, *Chem. Asian J.*, 2019, **14**, 1667–1671.
104 K. Becker, P. G. Lagoudakis, G. Gaefke, S. Höger and J. M. Lupton, *Angew. Chem., Int. Ed.*, 2007, **46**, 3450–3455.
105 K. Becker, G. Gaefke, J. Rolffs, S. Höger and J. M. Lupton, *Chem. Commun.*, 2010, **46**, 4686–4688.
106 H. Kawai, T. Umehara, K. Fujiwara, T. Tsuji and T. Suzuki, *Angew. Chem., Int. Ed.*, 2006, **45**, 4281–4286.
107 C. Schweez, P. Shushkov, S. Grimme and S. Höger, *Angew. Chem., Int. Ed.*, 2016, **55**, 3328–3333.
108 M. D. Cornelissen, S. Pilon, L. Steemers, M. J. Wanner, S. Frölke, E. Zuidinga, S. I. Jørgensen, J. I. van der Vlugt and J. H. van Maarseveen, *J. Org. Chem.*, 2020, **85**, 3146–3159.
109 K. Sugiyasu, Y. Honsho, R. M. Harrison, A. Sato, T. Yasuda, S. Seki and M. Takeuchi, *J. Am. Chem. Soc.*, 2010, **132**, 14754–14756.
110 C. Pan, K. Sugiyasu and M. Takeuchi, *Chem. Commun.*, 2014, **50**, 11814–11817.
111 C. Pan, K. Sugiyasu, Y. Wakayama, A. Sato and M. Takeuchi, *Angew. Chem., Int. Ed.*, 2013, **52**, 10775–10779.
112 A. Leventis, J. Royakkers, A. G. Rapidis, N. Goodeal, M. K. Corpinot, J. M. Frost, D. K. Bučar, M. O. Blunt, F. Cacialli and H. Bronstein, *J. Am. Chem. Soc.*, 2018, **140**, 1622–1626.
113 J. Terao, H. Masai, T. Fujihara and Y. Tsuji, *Chem. Lett.*, 2012, **41**, 652–653.
114 H. Masai, J. Terao, S. Makuta, Y. Tachibana, T. Fujihara and Y. Tsuji, *J. Am. Chem. Soc.*, 2014, **136**, 14714–14717.
115 H. Masai, M. Liu, Y. Tachibana, S. Tsuda and J. Terao, *J. Org. Chem.*, 2020, **85**, 3082–3091.
116 J. Terao, A. Wadahama, A. Matono, T. Tada, S. Watanabe, S. Seki, T. Fujihara and Y. Tsuji, *Nat. Commun.*, 2013, **4**, 1691.
117 H. Masai, T. Yokoyama, H. V. Miyagishi, M. Liu, Y. Tachibana, T. Fujihara, Y. Tsuji and J. Terao, *Nat. Commun.*, 2020, **11**, 408.
118 D. R. Paulson, S. B. Bhakta, R. Y. Hyun, M. Yuen, C. E. Beaird, S. C. Lee, I. Kim and J. Ybarra Jr., *Inorg. Chim. Acta*, 1988, **151**, 149–152.
119 H. Masai, J. Terao, S. Seki, S. Nakashima, M. Kiguchi, K. Okoshi, T. Fujihara and Y. Tsuji, *J. Am. Chem. Soc.*, 2014, **136**, 1742–1745.
120 T. Hosomi, H. Masai, T. Fujihara, Y. Tsuji and J. Terao, *Angew. Chem., Int. Ed.*, 2016, **55**, 13427–13431.